

Adaptable Gaussian Bases for Quantum Dynamics of the Nuclei

Sophya Garashchuk

Abstract Compactness of the wavefunction representation is one of the central practical question in quantum dynamics of high-dimensional molecular systems, because, for general inter-particle interactions, the complexity of a wavefunction grows exponentially with the system size. While expanding the wavefunctions in terms of standard pre-defined basis sets is well established in the electronic structure theory and computations, it is not so in the quantum dynamics of the nuclei. One 'family' of approaches is based on Gaussian functions whose parameters are tailored in some way to the shape of a wavefunction evolving in time, or to the energy and spatial range relevant to the system of interest; the choice of the basis parameters often comes from classical dynamics, semiclassical arguments or from coupled variational equations, all with their pros and cons. In this chapter we review in detail several approaches to constructing compact Gaussian bases, scalable to multidimensional systems and, in principle, yielding exact quantum dynamics: thawed Gaussian wavepacket dynamics, time-independent quasirandom distributed Gaussian bases and time-dependent Gaussian bases guided by quantum trajectories. The non-variational character of these methods and their adaptability to target wavefunctions, combined with recent advances in the on-the-fly electronic structure calculation, make them practical for applications to large molecular systems.

1 Introduction

Classical mechanics often gives adequate representation of the nuclei in molecular dynamics simulations. Yet, the nuclear quantum-mechanical effects (NQEs) may play a significant role in chemical and physical processes a wide range of molecular environments from the hydrogen storage within the metal-organic frameworks [1], to photovoltaic or spin-responsive materials [2, 3, 4], to enzyme activity [5]. The

Sophya Garashchuk
University of South Carolina, Columbia, SC 29208, USA, e-mail: garashchuk@sc.edu

NQEs are typically the largest for light nuclei at low temperatures and energies, or more specifically when the characteristic energy of a process is comparable to the separation between the vibrational energy levels of chemical bonds.

The most general description of NQE comes from a solution to the time-dependent Schrödinger equation (**TDSE**), possibly, with the time-dependent potential,

$$\hat{H}\psi(x,t) = i\hbar \frac{\partial}{\partial t} \psi(x,t). \quad (1)$$

The Hamiltonian operator is a sum of the kinetic and potential energy operators, \hat{K} and \hat{V} , the latter is a function of coordinates and time,

$$\hat{H} = \hat{K} + V(x,t), \quad \hat{K} = -\frac{\hbar^2}{2} \nabla^T \mathbf{M}^{-1} \nabla = -\frac{\hbar^2}{2} \sum_{n=1}^d \frac{1}{m_n} \frac{\partial^2}{\partial x_n^2}. \quad (2)$$

Throughout this chapter we consider SE only for the nuclei, evolving on a single electronic potential energy surface (**PES**). For simplicity, we will describe the nuclei in Cartesian coordinates (unless indicated otherwise) with the diagonal kinetic energy operator. In other words, \mathbf{M} is the diagonal matrix of the particle masses, $M_{nn} = m_n$, where index n enumerates the degrees of freedom (**DOFs**). Each particle is described by three coordinates in Cartesian space listed in a single vector x . The total number of DOFs (and the size of the vectors and matrices) is $d = 3 \times$ (number of particles). The atomic unit of the Planck's constant, $\hbar = 1$, is used henceforth. We will drop time as the argument in the external potential, $V \equiv V(x)$ with understanding that all methodologies described below, except those based on diagonalization of the Hamiltonian matrix of Section 3, are applicable to time-dependent potentials.

Computational efforts of describing a general quantum system, fully coupled by anharmonic interactions, scale exponentially with the system size. Therefore, efficient basis representation of wavefunctions is essential for the studies of high-dimensional molecular systems. While representation of wavefunctions in terms of standard bases is well established in the electronic structure theory, it remains an outstanding challenge in quantum mechanics of nuclei. This situation may be attributed to several factors.

- (i) The classical description of nuclei is adequate in many situations (molecular dynamics is very useful). Therefore, quantum molecular dynamics has not received as much attention from theorists as the electronic structure.
- (ii) The NQE are very sensitive to the quality of the electronic PES on which the dynamics unfolds. Thus, the development of practical methods (including theory, hardware and software) of computing globally accurate PES was necessary before the NQE could be rigorously included.
- (iii) Finally, the forces acting between the quantum nuclei are complicated many-body interactions and the systems undergo large-amplitude motion (reaction dynamics, isomerization, diffuse vibrational states, highly excited vibrational states). Consequently, most multidimensional quantum dynamics approaches are fairly system-specific.

While there is a number of standard approaches to solve the time-dependent Schrödinger equation for the nuclei through explicit time-evolution of wavefunctions, such as the split-operator/Fast Fourier Transform and Chebyshev expansion of the Hamiltonian, or the Hamiltonian diagonalization (iterative schemes) [6, 7, 8, 9, 10], there is no standard approach of generating a wavefunction representation (beyond a few dimensions), which would remain accurate and practical in the course of dynamics.

The term *quantum dynamics* is often used to indicate that one is dealing with the Schrödinger equation for the *nuclei* as opposed to electrons, regardless of whether time-dependent or time-independent wavefunction is required to answer the question at hand. Formally, for time-independent interactions, the time-dependent and time-independent solutions to the SE contain equivalent information, and are related through the Fourier Transform. In other words, if a time-dependent solution $\psi(x, t)$ to the TDSE (1) is available at all times, one can extract *all* energy eigenstates $\chi(x, E)$ as the Fourier transform of $\psi(x, t)$ into the energy domain,

$$\chi(x, E) = \mathcal{N}_E \int_{-\infty}^{\infty} \psi(x, t) e^{iEt} dt, \quad (3)$$

where \mathcal{N}_E is the normalization constant. Vice versa, knowing all the eigenstates,

$$\hat{H}\chi(x, E) = E\chi(x, E), \quad (4)$$

one can reconstruct the time-evolution of *any* initial wavefunction $\psi(x, 0)$:

$$\psi(x, t) = \int_0^{\infty} dE \langle \chi(x, E) | \psi(x, 0) \rangle e^{-iEt}. \quad (5)$$

'All eigenstates' above means the ones that overlap with $\psi(x, 0)$; we omit discussion of degenerate eigenstates for simplicity. The integral in Eq. (5) implies integration over the states of the continuum spectrum and summation over the discrete eigenstates as appropriate for the problem.

The standard ways to represent a wavefunction (as a linear combination of fixed in time and space functions) are the finite basis representation (**FBR**) and the discrete variable representation (**DVR**). The eigenvalues of the Hamiltonian operator evaluated in FBR, traced to the variational minimization of the energy functional, give the upper bound on energy levels, a useful feature. The downside to FBR is the high cost of computing the matrix elements of the potential energy operator, especially if the basis functions are delocalized, and the dense character of the resulting Hamiltonian matrices. The DVR approach, introduced by Light in the 1980s [11, 12, 13] and reviewed in Ref. [14], is an elegant way of addressing both deficiencies of FBR. In DVR, which is equivalent to evaluation of integrals by quadrature over the related to it finite basis, the potential energy matrix is diagonal and the high energy regions of the coordinate space can be excluded. Thus the number of the PES evaluations is minimized, while the kinetic energy matrix remains fairly sparse. These two advantages in conjunction with the development of iterative diagonalization techniques, such as short iterative Lanczos [15, 16, 17] made the DVR

a method of choice when doing exact quantum dynamics for both vibrational and scattering calculations. Even to date the state-of-the-art vibrational calculations of spectroscopic accuracy (of a few wavenumbers) use DVR, sometimes in combination with FBR for selected coordinates. One of the most sophisticated calculations, performed by Viel and Leforestier [18] for HFCO, employed six-dimensional DVR of over 10^7 points, truncated by potential energy to about half a million points, to obtain about 150 accurate eigenstates. Even with all the advantages of DVR and a modest 10-point DVR per dimension in average, the sheer size of the basis, which scales exponentially with the number of dimensions d , makes exact full-dimensional description of systems of more than five atoms ($d \geq 9$) impractical.

The unfavorable scaling of the basis size with d motivates the development of the quantum dynamics approaches based on the correlated, in other words not on the direct-product type, bases. While in general the scaling of the wavefunction complexity is at least exponential with d , the hope is that practical methods of generating efficient bases might be developed if the questions addressed by calculations are narrowed in some sense. For example, instead of accurate calculation of a full wavefunction, one may target convergence of certain expectation values, of the energy levels within the limited range of energy, or of the correlation functions yielding spectra of medium resolution.

For high-dimensional problems, the central idea behind a manageable-size basis is to make it adaptable to the time-evolution of the target quantities. The most accomplished exact quantum method, used in many high-dimensional applications [19], is the multiconfiguration time-dependent Hartree method (**MCTDH**) [20, 21, 22, 23], where multidimensional wavefunctions are built as products of single-particle functions, contracted from a general basis. The MCTDH-like method, closely related to the scope of this chapter, is the variational multiconfiguration Gaussian (vMCG) approach [24, 25, 26], based on Gaussian basis functions, whose parameters are formally defined by the evolving wavefunction through the time-dependent variational principle.

As in electronic structure theory, one reason to use Gaussian bases in quantum dynamics is their mathematical properties, such as 'the product of two Gaussians is a Gaussian', localized functions, analytic integrals, Gaussian quadrature and Hermite polynomials. Another reason is that, unlike in the electronic structure (**ES**) theory, a Gaussian wavefunction (also a polynomial \times a Gaussian) solve the TDSE for parabolic, possibly time-dependent, potentials. The harmonic oscillator model is the foundation for the analysis of molecular vibrations (the normal mode analysis of ES codes), while a Gaussian function is a standard description of a localized in space particle, such as a nucleus, moving close to classical regime. Finally, the ever growing efficiency of the ES calculations, enabling molecular dynamics with on-the-fly or on-the-grid *ab initio* ES evaluations and advances in the PES construction (such as the product representation [27, 28] and fitting/interpolation methods [29, 30]) made evaluation of the potential matrix elements over a localized coordinate-space basis practical.

In this chapter we discuss Gaussian-basis methods of solving the time-independent and time-dependent SE for the nuclei. The same ideas could be used to solve the SE

for electrons, or for both nuclei and electrons. Extension to electrons may be desirable, for example, in the presence of the time-dependent electric field of a laser. We limit ourselves to exact quantum methods, though we note that there are numerous semiclassical methods (thawed [31], frozen [32], cellular [33] dynamics, the Herman-Kluk propagator [34], linearized semiclassical initial value representation [35]) based on representation of a wavefunction as superposition of Gaussians. Unlike exact QM methods, the semiclassical methods do not yield exact solutions of the SE in the limit of infinite basis. The remainder of this chapter is organized as follows. First, we review the Gaussian wavepacket (**GWP**) solution to the TDSE and describe a recent application to spectroscopy of NH_3 (Section 2). Then, we describe the *time-independent* Gaussian bases tailored to PES (Section 3) and the *time-dependent* Gaussian bases tailored to quantum dynamics of a wavefunction (Section 4). The concepts are illustrated by examples from our research, i.e. the quasirandom distributed Gaussian bases (**QDGB**) for the TISE and the quantum trajectory-guided Gaussian bases (**QTGB**) for the TDSE. Finally, we survey the 'intermediate' approaches employing the time-independent bases and wavefunction reexpansions at finite time intervals, adapted to the temporal changes of the wavefunction (Section 5). Section 6 concludes.

2 Evolution of a Gaussian wavepacket

To set the stage, first we review an analytic solution to the TDSE with the parabolic potential, i.e. the Gaussian wavepacket, in d dimensions, as it is a useful model for molecular vibrations, and an inspiration for a multitude of Gaussian-based exact and semiclassical methods of quantum dynamics. The solution (see for example Ref. [36]) is given in a compact matrix form for a d -dimensional system described in Cartesian coordinates,

$$\psi(x, t) = \mathcal{N} \exp\left(- (x - q_t)^T \mathbf{A}_t (x - q_t) + i p_t^T (x - q_t) + i s_t + \gamma_t\right), \quad (6)$$

where \mathcal{N} is the initial normalization constant, so that $\gamma_0 = 0$,

$$\mathcal{N} = \left(\frac{2^N \det \mathbf{A}_{\mathfrak{R}}|_{t=0}}{\pi^N} \right)^{1/4}. \quad (7)$$

The wavefunction evolves according to the Hamiltonian,

$$\hat{H} = -\frac{1}{2} \nabla^T \mathbf{M}^{-1} \nabla + V, \quad V = \frac{1}{2} x^T \mathbf{V}_2 x, \quad (8)$$

The matrix \mathbf{M} is a diagonal matrix of particle masses, while \mathbf{V}_2 is a real symmetric matrix defining a quadratic potential, whose minimum is at the origin of the coordinate system and is equal to zero. In Eq. (6) the parameters q_t, p_t are real d -dimensional vectors, s_t and γ_t are real scalar functions of time, indicated as the

subscript. The wavefunction is defined in terms of a *complex symmetric* matrix \mathbf{A}_t ,

$$\mathbf{A}_t = \mathbf{A}_{\Re} + i\mathbf{A}_{\Im}.$$

The subscript t is omitted for clarity when unambiguous. The vector ∇ is the gradient with respect to the particle coordinates, x .

Substituting Eq. (6) into the TDSE with the Hamiltonian (8), dividing the result by $\psi(x,t)$ and setting imaginary and real coefficients, multiplying powers of x , to zeroes, one obtains the following equations determining the time-evolution of the parameters:

$$\frac{dq}{dt} = \mathbf{M}^{-1}p, \quad \frac{dp}{dt} = -\nabla V(q), \quad (9)$$

$$\frac{ds}{dt} = \frac{p^T \mathbf{M}^{-1}p}{2} - V(q) - \text{Tr}(\mathbf{A}_{\Re}\mathbf{M}^{-1}), \quad (10)$$

$$i\frac{d\mathbf{A}}{dt} = 2\mathbf{A}\mathbf{M}^{-1}\mathbf{A} - \frac{1}{2}\mathbf{V}_2, \quad \frac{d\gamma}{dt} = \text{Tr}(\mathbf{A}_{\Im}\mathbf{M}^{-1}). \quad (11)$$

Note, that Eqs (9) are simply the Newton's equations of motion for the center of the Gaussian wavepacket, $q_t = \langle \psi|x|\psi \rangle_t$. Thus, (q_t, p_t) are the coordinates and momenta of a classical trajectory. Eq. (10) defines evolution of the classical action function s_t for the trajectory (q_t, p_t) , except for the last term on the RHS,

$$U_0 \equiv \text{Tr}(\mathbf{A}_{\Re}\mathbf{M}^{-1}).$$

This term does not affect the expectation values, but it does affect time-correlation functions and extracted from them spectra. U_0 can be interpreted as the zeroth order quantum effect, a time-dependent versions of the ZPE. In a special case of $\psi(x,t)$ being the ground state of the harmonic oscillator, U_0 is equal to the ground state energy E_0 , defining the trivial time-dependent phase of the ground state solution, $\psi(x,t) = \chi(x, E_0) \exp(-iE_0t)$.

Finally, the time-dependence of \mathbf{A} defines what is referred to as the breathing mode of the Gaussian, i.e. the change in localization of $|\psi(x,t)|$, with accompanying it quadratic phase. The changes in the real 'width' of a Gaussian define the time-dependence of the function γ_t , which ensures the constant in time wavefunction norm, $\langle |\psi(x,t)|^2 \rangle = 1$. Because of the 'breathing' motion of the wavepacket, superimposed on the classical motion of the Gaussian center, this solution to the TDSE is also known as the *thawed* Gaussian wavepacket (**TGWP**). The breathing mode is the next order quantum effect, specific to non-coherent Gaussian wavepackets. For a special choice of the initial wavefunction the width parameter \mathbf{A} remains constant in time, while the wavepacket center executes classical motion within the parabolic well. (This is the so-called *coherent* wavepacket: in the normal modes coordinates \mathbf{A} is diagonal, $A_{nn} = m_n\omega_n/2$, where ω_n and m_n are the frequency and mass of the n^{th} normal mode.) An analytic solution to \mathbf{A} is known for the harmonic oscillator [36], but in general, for the time-dependent V solutions of Eq. (11), determining the complex Gaussian width \mathbf{A} , are solved numerically using sophisticated propagators,

such as the Poisson propagator [37], to ensure stability. For the wavefunction to be normalizable, the eigenvalues of $\mathbf{A}_{\mathfrak{R}}$ have to be positive.

The total energy of ψ ,

$$E = \langle \psi | \hat{H} | \psi \rangle = \frac{1}{2} p^T \mathbf{M}^{-1} p + V(q) + \frac{1}{2^{d+1}} \text{Tr}(\mathbf{A}_{\mathfrak{R}}^{-1} \mathbf{V}_2) + \mathcal{U}, \quad (12)$$

consists of the classical energy of the wavepacket center (first two RHS terms) and, in addition, of the potential energy term due to the wavepacket delocalization (the third term in RHS of Eq. (12)). The last term, \mathcal{U} , is the kinetic energy associated with the derivatives of the wavefunction amplitude and phase, respectively,

$$\mathcal{U} = \frac{1}{2} (\text{Tr}(\mathbf{A}_{\mathfrak{R}} \mathbf{M}^{-1}) + \text{Tr}(\mathbf{A}_{\mathfrak{S}} \mathbf{A}_{\mathfrak{R}}^{-1} \mathbf{A}_{\mathfrak{S}} \mathbf{M}^{-1})). \quad (13)$$

The wavefunction ansatz of Eq. (6), approximating a time-dependent solution to SE for *anharmonic* potentials, i.e. TGWP [38, 39], found applications in spectroscopy. TGWP evolves on the potential, expanded up to the second order in x around the wavepacket center, which simply means dynamics in a quadratic potential with time-dependent parameters. Obvious limitations of this approach are the inability to describe the wavefunction bifurcation and interference effects within a single Gaussian ansatz, and inaccuracy of the quadratic expansion of V , when TGWP spreads in coordinate space. A more rigorous version of TGWP is the variational GWP [40]: the evolution equations for the wavepacket parameters are derived from the McLachlan variational principle [41]. The resulting equations for the GWP parameters involve the potential and its first and second derivatives averaged over the wavefunction, rather than their values at the center of the GWP of the TGWP. Both the variational and thawed GWP dynamics are valid either at short times or for nearly harmonic potentials, while the Gaussian function is accurate over the space relevant to the computed quantity.

The variational GWP has conceptual appeal, but beyond model applications, the thawed GWP (the local harmonic approximation to V) has a big advantage that the PES information is needed only along a single trajectory. The PES can be rather straightforwardly computed on-the-fly, as demonstrated in recent applications to spectroscopy of floppy molecules from the Vanicek group [42, 43]. The authors have used the TGWP dynamics, while computing the PES, its gradient and the Hessian on-the-fly (needed to solve Eqs (9), (10) and (11)) to analyze the emission spectroscopy of oligothiophenes and absorption and photoelectron spectra of ammonia. What is remarkable in these applications is that the ES has to be solved for along a single trajectory, which enabled efficient modeling of the oligothiophenes consisting of 2,3,4 and 5 rings. The latter system involves dynamics of 105 DOFs, carried out up to 0.2 ps. The TGWP emission spectra agree the experimental ones quite well as shown in Fig. 1: the peak structure is reproduced, although there is an overall shift in peak positions. This shift may be attributed to the theory – local harmonic approximation of the PES, quality of the electronically excited PES com-

puted using the Density Functional Theory, specifically CAM-B3LYP/6-31+G(d,p), or to the experimental conditions, i.e. interaction with the solvent.

For ammonia, the TGWP dynamics on the ground electronic PES, yielded medium resolution photoelectron and absorption spectra in good agreement with experiments, despite the limitations of a Gaussian wavefunction form. This is surprising because the inversion of NH_3 (the 'umbrella' mode) is characterized by the double-well potential, typical for floppy molecules, and the local harmonic representation of the PES is a big approximation in this case. The TGWP description was reasonably accurate for up to 0.2 ps, yielding the medium resolution spectra, though the accuracy of dynamics was insufficient for longer times, when the wavepacket bifurcates, to obtain the higher spectral resolution. The ab initio on-the-fly TGWP setup also enabled useful mode decomposition analysis. For example, for the two thiophene ring system (system T2 in Fig. 1) 8 effective modes, comprised of 42 DOFs in full dimension, were identified as contributing to the emission spectrum. This type of analysis gives insight into the mode coupling and also paves the way for more accurate quantum dynamics studies in reduced dimensionality.

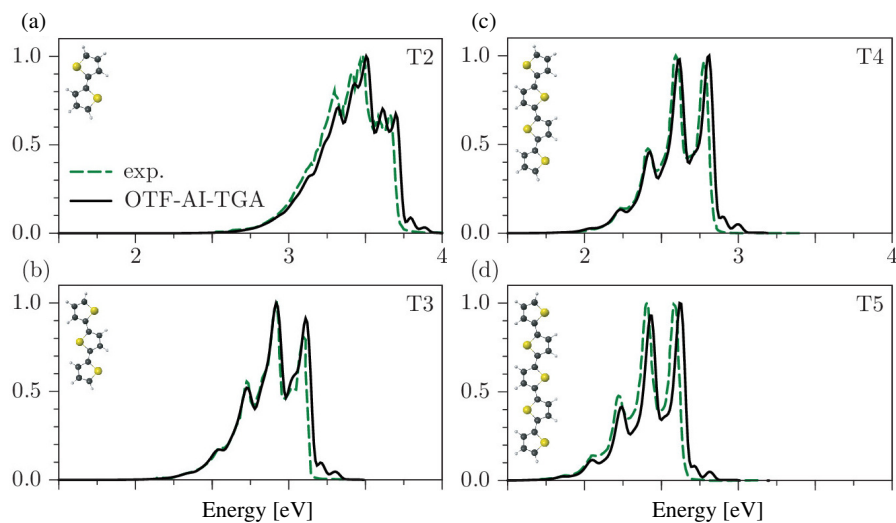


Fig. 1 Emission spectra of the oligothiophene chains T_n for $n = \{2, 3, 4, 5\}$ shown in panels (a-d), respectively. The experimental emission spectra (exp., dashed green line) is compared with the full-dimensional TGWP calculations, which includes all normal modes (solid black line). The excited electronic energy, its gradient and Hessian are computed on-the-fly ab initio (OTI-AI) using CAM-B3LYP density theory functional. Adapted with permission from Ref. [42]. Copyright 2014 American Institute of Physics.

All-in-all, a single complex TGWP gives a very efficient description of 'mild' quantum effects (before the wavefunction bifurcates and quantum interference becomes important) and is useful in certain spectroscopic applications. In more challenging applications, the TGWPs have been used to represent passive (spectator or

bath) modes characterized by the mild quantum effects in combination with more accurate basis representations for the active (reactive or subsystem) modes, such as in the multilayer Gaussian-MCTHD method [44, 45]. The simplicity and elegance of TGWP inspired numerous approximate and semiclassical dynamics methods, based on expansion of a wavefunction or a propagator in terms of Gaussian functions. The common feature of these methods is that they are based on classical trajectory motion with the quantum effects incorporated from additional information, such as the trajectory action function and monodromy or stability matrix elements related to the width matrix \mathbf{A} of TGWP. Some of the most popular semiclassical methods are based on representation of a wavefunction or a propagator in terms of integrals (over the initial trajectory positions, momenta or both) of Gaussians [46, 33, 34, 47, 48, 35, 49, 50]. An interesting recent methodology aims to reduce the semiclassical propagation error by 'slicing' the total propagation into short segments over which the Gaussians are evolved analytically, and reexpanding the wavefunction in a new set of Gaussians [51]. Another impact of the TGWP approach on quantum dynamics as a field, is in the use of classical mechanics arguments, i.e. energy and phase space analysis, to construct compact efficient basis representations for exact QM dynamics approaches, including time-independent, time-dependent and 'intermediate' methodologies, discussed and illustrated below.

3 Time-independent Gaussian bases adapted to PES

In this section we review construction of efficient basis representation of the vibrational states employing Gaussian functions whose parameters are tuned to the features of the PES. Most of Section 3 is adapted with permission from [S. Garashchuk and J. C. Light, Quasirandom distributed Gaussian bases for bound problems, *J. Chem. Phys.*, 114:3929–3939, 2001] Copyright 2001 American Institute of Physics.

Construction of a compact (in a sense of the number of functions) correlated basis for solving the time-independent SE, is especially important for studies of highly excited vibrational states of polyatomic molecules or molecular clusters, corresponding to the large amplitude intermolecular motion. To construct a basis for such problems, Davis and Heller [52] considered complex Gaussian basis sets distributed in phase space through the Wigner distribution, though later it has been demonstrated that real distributed Gaussian basis sets (**DGBs**) [53] performed as well or better. In the latter approach the distance between neighboring Gaussians was made proportional to the local de Broglie wavelength, and the exponents adjusted to give a desired average overlap of the (non-orthogonal) basis functions. The DGB representation, usually for the radial DOFs in conjunction with the DVRs in angles, was found efficient for a number of triatomic systems [54, 55, 56, 57, 58, 59]. A later one-dimensional (**1D**) study of the *fully optimized* variational Gaussian bases [60] has shown that higher accuracy of the Hamiltonian eigenvalues was observed for very small reciprocal condition number (**RCN**) η . Small η , defined as the ratio of

the smallest to largest eigenvalues of the overlap matrix \mathbf{S} , typically signals the linear dependence in the basis, but the strongly overlapping functions (responsible for small values of η) give better description of the wavefunction derivatives. The full basis optimization of Ref. [60] is a nonlinear problem, which scales as the number of basis functions N_b to the *fifth* power, making it impractical for multidimensional systems. In this section we review the subsequent development of the quasirandom distributed Gaussian bases (QTGB) [61], which are not optimized, but incorporate features of the optimal bases known from the 1D studies, including the small RCN. The QTGB performance is illustrated on calculations of the rovibrational energy levels of H₂O.

3.1 Optimized Distributed Gaussian Bases

Our goal here is to construct an efficient basis comprised of real normalized Gaussians, $\{g_i\}$, $i \in [1, N_b]$,

$$g_i = \left(\frac{2\alpha_i}{\pi} \right)^{1/4} \exp(-\alpha_i(x - q_i)^2), \quad (14)$$

which can accurately represent the vibrational states whose energies are below a certain cutoff value, E_{cut} . For clarity of presentation, we will consider a Cartesian-space Hamiltonian with separable kinetic energy given by Eq. (2), and outline the procedure in one dimension, x . The Gaussian basis is not orthogonal, thus, to find the eigenstates of \hat{H} we need to compute the overlap matrix \mathbf{S} with the elements

$$S_{ij} = \langle g_i | g_j \rangle, \quad (15)$$

the Hamiltonian matrix \mathbf{H} with the elements,

$$H_{ij} = \langle g_i | \hat{H} | g_j \rangle, \quad (16)$$

and to solve the generalized eigenvalue problem for the matrix pair (\mathbf{H}, \mathbf{S}) :

$$\mathbf{H}\mathbf{B} = \mathbf{S}\mathbf{B}\mathbf{E}. \quad (17)$$

The diagonal matrix \mathbf{E} contains the energy eigenvalues, while the columns of the matrix \mathbf{B} are the respective eigenvectors. The basis function overlaps and the matrix elements of the kinetic energy operator are evaluated analytically. The potential matrix elements,

$$V_{ij} = \langle g_i | V | g_j \rangle, \quad (18)$$

can be efficiently computed using low-order Gauss-Hermite quadrature or local quadratic approximation to $V(x)$, taking advantage of the product property of Gaussians and provided that the Gaussian basis functions are sufficiently localized.

The kinetic energy associated with each g_i is proportional to its width parameter, $K_{ii} = \alpha_i/(2m)$. Thus, given the energy cutoff E_{cut} , a reasonable expectation is that the optimal value of α_i is related to the 'residual' kinetic energy at the basis function center,

$$\alpha_i \sim m(E_{cut} - V(q_i)). \quad (19)$$

As shown in Ref. [53], according to the semiclassical arguments, the density of the Gaussian centers should be proportional to the particle momentum, while according to numerical tests, use of the kinetic energy instead,

$$\rho(q_i) = \frac{1}{2(q_{i+1} - q_{i-1})} \sim (E_{cut} - V(q_i)). \quad (20)$$

gives more accurate results. Both options generate the basis functions that are narrower in the regions of low V (or higher kinetic energy), thus distribution of $\{q_i\}$ can be made denser in those regions; in the regions of high V (low kinetic energy) the basis functions can be broader and placed further apart.

To develop cheap procedure of specifying the positions $\{q_i\}$ and width $\{\alpha_i\}$, as an alternative to the full variational optimization [60], we have analyzed optimal solutions to the following functional, \tilde{F} ,

$$\tilde{F} = \text{Tr}(\mathbf{H}) - \lambda \sum_{i,j,i \neq j} \frac{S_{ij}}{1 - S_{ij}}. \quad (21)$$

The functional is minimized with respect to all q_i and α_i (without assumptions on their functional forms). The functional includes the energy term as the trace of \mathbf{H} and the basis function 'repulsion' term controlled by the parameter λ . If the basis is orthogonal, the second term is equal to zero and \tilde{F} reduces to the trace of the Hamiltonian matrix. For a non-orthogonal basis, minimization of the $\text{Tr}(\mathbf{H})$ term alone would yield N_b copies of the ground state, $\text{Tr}(\mathbf{H}) = N_b E_0$. The role of the repulsion term is to prevent large off-diagonal overlaps S_{ij} leading to the linear dependence in a basis, i.e. the degeneracy of \mathbf{S} . During minimization of \tilde{F} the parameter λ was set to a fixed value, but we found that accuracy of the eigenstates could be further improved by *uniform* scaling of α_i , which lowers the Hamiltonian eigenvalues. Thus, the procedure may be viewed as a two-step minimization of \tilde{F} : (i) optimize the Gaussian parameters for fixed λ ; (ii) 'tune' the basis by uniform rescaling of $\{\alpha_i\}$ to lower the energy term, $\text{Tr}(\mathbf{H})$; the rescaling factor effectively controls the Gaussian repulsion strength, which is the role of the parameter λ in Eq. (21).

The results of the simplified basis optimization above have been analyzed for several 1D models with the goal of identifying any trends usable in realistic multidimensional problems. In particular, the two-step minimization has been used to compute all bound energy levels of a 1D Morse oscillator for a particle of mass $m = 1$,

$$V(x) = D (\exp(-wx) - 1)^2, \quad (22)$$

which is 'potential B' from Ref. [53]. The parameter values are $D = 12.0 E_h$ and $w = 0.2041241 a_0^{-1}$; there are 24 energy levels below D . On the far right the potential

is set to $V(x) = 25.0 E_h, x > 70 a_0$. The nonlinear minimization procedure converged for the range of repulsion strength $\lambda = [0.5, 1.5]$, yielding the expected behavior of the optimal Gaussian density and width, shown in Fig. 2. For $\lambda = 1$, the obtained RCN of the overlap matrix was $\eta \approx 10^{-5}$. Thus, we could fully explore the effect of the basis wavefunction broadening the basis functions. Scaling of all α_i by a constant, towards $\eta = [10^{-9}, 10^{-12}]$, *increased* the accuracy of the energy levels by about three orders of magnitude. For yet smaller values of η the eigenvalues of \mathbf{H} increased. Similar relation of the accuracy on RCN has been seen in other model systems (see Ref. [61] for more details), leading to a conclusion that there is a sizable optimal range of η spanning 2 – 4 orders of magnitude yielding low eigenenergies.

Figure 3 compares the highest bound eigenfunction computed in a basis to the analytic eigenfunction. The agreement is excellent and, given the diffuse nature of this eigenstate, the basis is highly efficient: all energy levels were obtained within the relative accuracy of 10^{-5} , using only two basis functions per eigenstate, $N_b = 48$. The best accuracy has been achieved by scaling the optimized widths $\{\alpha_i\}$ by 0.13, yielding RCN of $\eta = 1.47 \times 10^{-13}$. Another important observation is that the optimized widths and density could be accurately represented as linear functions of $V(x)$, as seen in Fig. 2.

Overall, according to the model analysis of the nonlinear minimization of \tilde{F} , we conclude that while the full optimization of the basis parameters is impractical in high dimensionality, efficient correlated basis can be simply constructed by introducing the linear dependence of the basis function widths on the kinetic energy, $\alpha_i = c(E_{cut} - V(q_i))$, followed by the uniform scaling of α_i to shift the RCN of the overlap matrix towards the range $\eta \sim 10^{-8} - 10^{-10}$. Then, the only two features of the basis, left to be tested directly, are the width scaling factor c and the basis size.

Fig. 2 The widths, $\{\alpha_i\}$, and the density $\{\rho_i\}$ of Gaussians as a function of their centers, $\{q_i\}$, for the Morse oscillator: circles mark α_i found from the minimization of the functional \tilde{F} , Eq. (21); solid line is the fit of α_i with the linear function of the potential; squares mark the optimized density and the dashed line is its linear fit. Adapted with permission from Ref. [61]. Copyright 2001 American Institute of Physics.

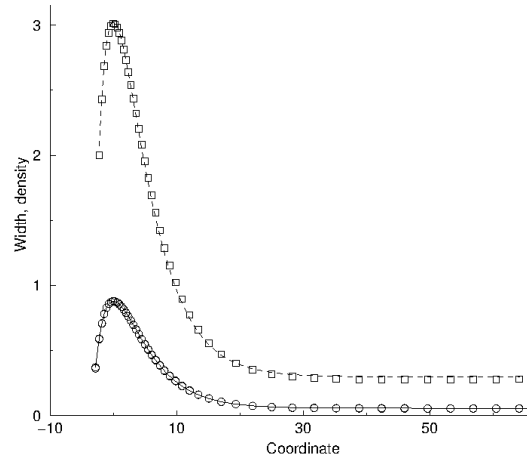
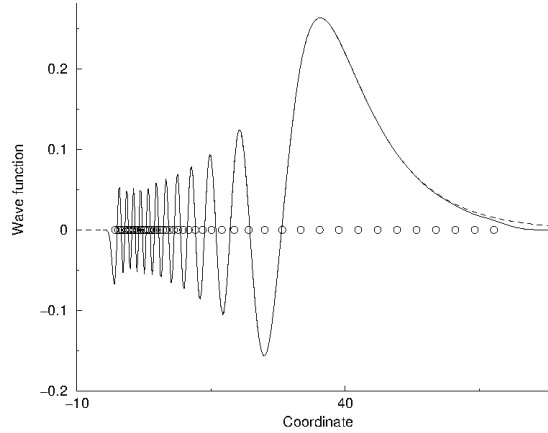


Fig. 3 The eigenfunction of the highest, $n = 23$, energy level for the Morse potential in coordinate space: dashed line shows the analytic result and the solid line shows the numerical eigenfunction. The centers of basis functions (circles) are also shown. Adapted with permission from Ref. [61]. Copyright 2001 American Institute of Physics.



3.2 Quasirandom distributed Gaussians

For high-dimensional problems, the full nonlinear optimization of Section 3.1 becomes expensive, if feasible at all. Thus, to generate a PES-adapted basis, we simply use the linear in V functional form of the basis function parameters to accomplish two tasks.

The first task is to place the Gaussian centers achieving the desired distribution of their centers. We use a quasirandom sequence to generate the Gaussian basis functions with potential-dependent density and widths within the energy contour $V(x_i) < E_{cut}$. A general real Gaussian in d -dimensional coordinate space is

$$g_i(x) = \mathcal{N}_i \exp\left(-(x - q_i)^T \mathbf{A}_i (x - q_i)\right), \quad (23)$$

where the normalization constant \mathcal{N}_i is given by Eq. (7) for $\mathbf{A} = \mathbf{A}_i$. The width parameters are arranged as a real symmetric matrix \mathbf{A}_i , in general, with nonzero off-diagonal elements and positive eigenvalues. Here we take \mathbf{A}_i as a diagonal matrix $A_{in} = \alpha_{in}$, where n enumerates dimensions and i enumerates the basis functions.

The second task is to choose the Gaussian width parameters according to Eq. (19),

$$\alpha_{in} = cm_n (E_{cut} - V(q_{in}) + \Delta), \quad n = 1 \dots d \quad (24)$$

with the same value of c for all basis functions and all dimensions. Guided by the results of full optimization in 1D of Section 3.1, the scaling parameter c is adjusted to have the reciprocal condition number in the range $\eta = [10^{-6}, 10^{-14}]$. The density of centers is also a linear function of the potential

$$\rho(q_i) \sim E_{cut} - V(q_i) + \Delta. \quad (25)$$

In Eqs (19) and (25) we have introduced a parameter Δ , affecting the ratio of the largest to smallest width parameter. Thus, Δ controls the sensitivity of the basis

function to the PES. In the limit of large Δ , $\Delta \gg E_{cut}$ the Gaussians will have nearly equal width. Small values of Δ , $\Delta < E_{cut}$, will generate a basis whose center density and width are sensitive to the potential and mimic the optimal basis of Section 3.1. The scaling parameter c is chosen to minimize the sum of the energy eigenvalues. The value of c can be estimated from the lowest eigenvalue as

$$c \sim \frac{2E_0}{E_{cut} \sum_n m_n},$$

or better yet, from the normal modes vibrational analysis at the minimum of $V(x)$. Another option is to adjust both parameters, c and Δ , by computing a few eigenstates for a low E_{cut} in a small-sized QDGB, and then use those values for the target energy range (large E_{cut}). Overall, for a predetermined energy cutoff E_{cut} , the procedure has two adjustable parameters, c and Δ , and generates an efficient, correlated multidimensional basis in the coordinate space.

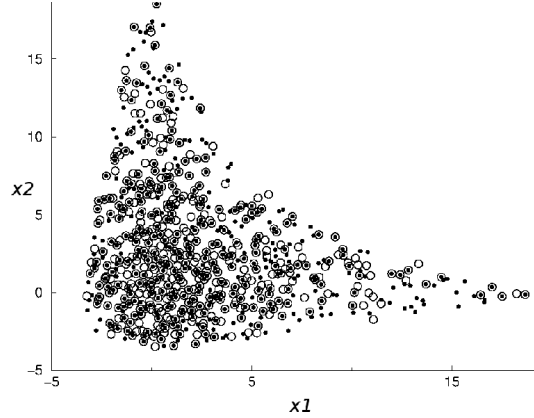
Placing Gaussian basis functions according to the desired density of their centers $\rho(x)$ is accomplished by accepting randomly generated positions with the probability proportional to $\rho(x)$. In addition, to avoid excessive linear dependence in the basis, the new function is rejected if its maximal overlap with previously accepted functions exceeds certain threshold. In fact, quasirandom or sub-random sequences of numbers are more efficient for our purposes. The quasi-random sequence has the advantage that the points q_i are generated as far apart as possible given the previous points in the sequence. For a relatively sparse distribution of points, this feature significantly reduces the probability that two points are so close to each other that one of them is rejected according to the Gaussian overlap criterion. The convergence of the energy eigenvalues with respect to the number of basis functions N_b can be monitored while the sequence of Gaussian centers q_i is being generated.

We use the Sobol sequence to generate the quasirandom points, and their density is modified according to Eq. (25) with the *rejection* method [62]. The point q_i is accepted if

$$\left[\frac{E_{cut} - V(q_i) + \Delta}{E_{cut} + \Delta} \right] > b_i, \quad (26)$$

where numbers $b_i = [0, 1]$ belong to an independent sequence of random (not quasirandom) numbers. This basis is referred to as the non-uniform, i.e. width and density are adapted to PES, quasirandom distributed Gaussian basis or QDGB. For illustration, the positions of Gaussian centers adapted to a 2D Morse oscillator potential are plotted in Fig. 4. The 122 energy eigenstates, with the eigenvalues below 95% of the dissociation energy, were computed using 482 functions, within the relative error of less than 10^{-4} .

Fig. 4 The centers of the non-uniform QDGB 482 functions for the 2D Morse oscillator. The two sets, motivated by the 1D optimization, $\rho \sim E_{cut} - V(q) + \Delta$, and by the 1D semiclassical de Broglie wavelength, $\rho \sim (E_{cut} - V(q) + \Delta)^{1/2}$, are shown with open and filled circles, respectively. Adapted with permission from Ref. [61] Copyright 2001 American Institute of Physics.



3.3 Calculation of the energy levels for triatomic molecules

3.3.1 Water molecule

As a chemically-relevant demonstration of the QDGB generation scheme and performance we have calculated the vibrational energy levels of water for the total angular momentum $J = 0$ using the potential energy surface of Ref. [63]. The target convergence of the energy levels below 25118 cm^{-1} (252 states in all) was the 'spectroscopic' accuracy of 0.1 cm^{-1} .

We have used the triatomic vibrational Hamiltonian in Radau coordinates, which allows analytic evaluation of the kinetic energy operator,

$$\hat{H} = K^{2D} + K^\theta + V(R_1, R_2, \theta). \quad (27)$$

The two-dimensional kinetic energy for the distance variables is

$$K^{2D} = -\frac{\hbar^2}{2m_1R_1^2} \frac{\partial}{\partial R_1} \left(R_1^2 \frac{\partial}{\partial R_1} \right) - \frac{\hbar^2}{2m_2R_2^2} \frac{\partial}{\partial R_2} \left(R_2^2 \frac{\partial}{\partial R_2} \right). \quad (28)$$

The angular part of the Hamiltonian is

$$K^\theta = -\frac{\hbar^2}{2} \left(\frac{1}{m_1R_1^2} + \frac{1}{m_2R_2^2} \right) \mathbf{j}^2, \quad (29)$$

where

$$\mathbf{j}^2 = \frac{1}{\sin \theta} \frac{\partial}{\partial \theta} \left(\sin \theta \frac{\partial}{\partial \theta} \right). \quad (30)$$

The volume element is $R_1^2 R_2^2 \sin \theta dR_1 dR_2 d\theta$ [56, 64]. The QDGB is used to describe the distance variables, R_1 and R_2 ; the Legendre DVR is used to represent the angle θ . In the DVR the potential matrix is diagonal with respect to the discretized

angle variable θ . Thus we construct angle-specific two-dimensional Gaussian bases $\{g^{(\mu)}\}$ for the two-dimensional Hamiltonians for each value, θ_μ [54, 64],

$$H_\mu^{2D} = K^{2D} + V(R_1, R_2, \theta_\mu). \quad (31)$$

The 2D Hamiltonians for different θ_μ are coupled via K^θ terms with the DVR expression for the \mathbf{j}^2 operator [65, 66]. The kinetic energy matrix elements are integrated on the range of the distance variables, i.e. $R_{1(2)} \in [0, \infty]$. The Gauss-Hermite quadrature of low order (4-7 points) is employed to compute the potential matrix elements. The 2D bases consist of Gaussians of variable width distributed quasi-randomly within the energy contour E_{cut} as described in Section 3.2. The width parameter of i -th Gaussian centered at (R_{i1}, R_{i2}) is scaled by the masses m_1 and m_2 ,

$$\alpha_{i1(2)} = cm_{1(2)}(E_{cut} - V(R_{i1}, R_{i2}) + \Delta). \quad (32)$$

The optimal value of c is found from a one-dimensional scan of the trace of H^{2D} over the values of c . The convergence of the energy levels below E_{cut} is monitored during the construction of the basis. For each angle θ_μ , the size of the 2D Hamiltonian matrix is reduced by the number of eigenvalues above the truncation energy, E_{tr} . Then, the appropriately transformed angular kinetic energy K^θ is added to the diagonalized H_μ^{2D} ; the resulting matrix, truncated according to the energy cutoff E_{tr} forms the μ^{th} block of the full Hamiltonian matrix.

The numerical parameters for ten different QDGB/DVR calculations, performed to test the convergence and relative importance of various details of the setup, are listed in Table 1. The parameter Δ of Eq. (32) equals to $0.01 E_h$ ($\approx 1800 \text{ cm}^{-1}$) for all calculations. The 2D QDGB sets were constructed by adding 20 functions at-a-time and their widths scaled. The smallest tolerated RCN was $\eta = 10^{-13}$. The basis size was fixed once either the target accuracy of the eigenvalues was met (in 2D) or until the number of functions exceeded 300. The number of Gaussian basis functions and the matrix size after the truncation are shown in Fig. 5 for the basis IV. On average, the truncation procedure reduces the basis size by 60%. For several angles the target convergence of the 2D eigenvalues (better than 1 cm^{-1}), is not met. However, all levels below 32000 cm^{-1} are converged within 1.3 cm^{-1} , and those below 30000 cm^{-1} are converged within $< 0.55 \text{ cm}^{-1}$. Since there are few 2D eigenvalues below E_{tr} at small angles, E_{cut} was increased for $\theta < 39^\circ$, so that at least 40 QDGB functions are generated. The total matrix size of the full 3D calculations varied from 1574 to 3551. The symmetry of the molecule was not taken into account.

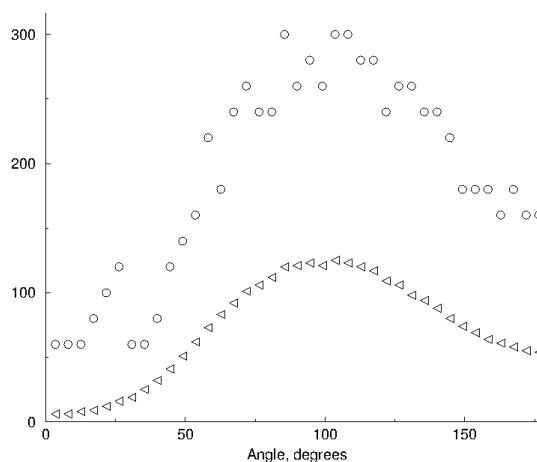
The dependence of the energy levels on (i) the initial seed of the random sequence $\{b_i\}$ of Eq. (25), (ii) on the number of the quadrature points for R_1 and R_2 and (iii) on the eigenvalue truncation energy parameter is illustrated in Table 1. The table shows the maximal deviation among N_l lowest levels from the energy levels obtained from our largest, most accurate calculation employing basis I. The number of levels, $N_l = \{400, 350, 300, 250, 200\}$ correspond to the energies of $\{29520, 28183, 26714, 25069, 23153\} \text{ cm}^{-1}$, respectively. The number of levels obtained with the bases II, III and IV that differ from the levels of the largest calcu-

Table 1 Convergence of the energy levels for the H₂O molecule for various QDGBs. The listed basis parameters are: N_θ is the number of angular DVR points; N_q is the number of quadrature points per dimension for radial integrals; E_{tr} (E_h) is the truncation energy for the 2D eigenvalues; E_{cut} (E_h) is the cutoff energy for the placement of Gaussians; ϵ (cm^{-1}) is the convergence criterion for energy levels, used to construct 2D QDGB; N_{max} is the total size of the truncated matrix. The largest deviation for energy levels of water in cm^{-1} (taking those of the largest QDGB I as a reference), is listed for the lowest N_i eigenvalues. Adapted with permission from Ref. [61] Copyright 2001 American Institute of Physics.

basis	Basis parameters						Maximal deviation [cm^{-1}]					
	N_θ	N_q	E_{tr}	E_{cut}	ϵ^{2D}	N_{max}	N_i	400	350	300	250	200
I	43	5	.23	.165	1.0	3551	—	—	—	—	—	—
II	39	5	.23	.165	1.0	3232	0.43	0.35	0.17	0.08	0.03	
III	43	5	.22	.16	1.0	3129	1.02	0.33	0.18	0.07	0.02	
IV	39	5	.22	.16	1.0	2834	0.62	0.42	0.09	0.05	0.03	
V	39	5	.23	.16	1.0	3198	0.60	0.41	0.09	0.05	0.03	
VI	39	7	.22	.16	1.0	2838	0.64	0.43	0.11	0.07	0.03	
VII ^a	39	5	.22	.16	1.0	2777	8.38	3.76	1.90	0.50	0.09	
VIII ^b	39	5	.22	.16	1.0	2838	0.73	0.34	0.10	0.06	0.03	
IX	39	5	.20	.15	2.0	2138	6.02	3.80	1.26	0.31	0.12	
X	39	4	.18	.145	2.0	1574	12.29	4.70	2.50	0.87	0.24	

^a small angles are excluded; ^b different seed for the random sequence $\{b_i\}$ in Eq. (26) is used

Fig. 5 Water molecule eigenstate calculation: the size of the 2D basis before and after truncation procedure as a function of the DVR angle. Adapted with permission from Ref. [61]. Copyright 2001 American Institute of Physics.



lation by less than 1.0, 0.5, 0.2, 0.1 and 0.05 cm^{-1} is shown in Table 2: for the most efficient basis 7 basis per energy level were required to achieve convergence below one wavenumber.

To briefly summarize this section, the non-uniform QDGB are found to be accurate and efficient, with good convergence properties. The obtained energy levels agree with those of Ref. [63] to sub-wavenumber accuracy; the highest energy reported in Ref. [63] ($n = 252$) is *higher* than its counterpart in the QDGB calculation by 0.6 cm^{-1} . The non-uniform QDGB, being fully adaptable to the PES, including the functions' density and width, is more efficient than the equal-width Gaussian

Table 2 The number of levels converged to a specified accuracy in calculations with bases II, III and IV. The bases are described in Table 1. The convergence is defined with respect to the basis I calculation. Adapted with permission from Ref. [61] Copyright 2001 American Institute of Physics.

Accuracy [cm^{-1}]	1.02	0.50	0.20	0.10	0.05
Number of levels	413	378	321	292	211
Highest energy level [cm^{-1}]	29785	28908	27357	26489	23552

bases used in Ref. [56]. More challenging applications of the QDGB to the neon and argon trimers [61] support the overall conclusion on the QDGB performance.

4 Time-dependent Gaussian bases adapted to the wavefunction dynamics

We start this section with a review of the basic features of solving the TDSE within a time-dependent basis representation of a wavefunction, as well as some of the established dynamics approaches. Then, the concept of the quantum trajectory dynamics is outlined and combined with the semiclassical idea of frozen Gaussians [32], to yield a formally exact dynamics employing the *quantum-trajectory* guided Gaussian bases (**QTGB**). Model applications and discussion conclude the section. Most of Section 4 is adapted with permission from [B. Gu and S. Garashchuk, Quantum Dynamics with Gaussian Bases Defined by the Quantum Trajectories, *J. Phys. Chem. A*, 19:3023–3031, 2016]. Copyright 2016 American Chemical Society.

4.1 The formalism

A general approach to solving the TDSE (1), is to represent a wavefunction in a, possibly, non-orthogonal basis of N_b functions, $\{g_i(x,t)\}$, $i \in [1, N_b]$. At time t , a wavefunction is expressed in terms of these basis function,

$$\psi(x,t) = \sum_{i=1}^{N_b} c_i(t) g_i(x,t), \quad (33)$$

where $\{c_i(t)\}$ are the expansion coefficients. The positions of all particles are specified by the vector x of length d (the number of DOFs). Let us assume that the i^{th} basis function depends on time only through the time-dependent parameters enumerated by the index $\mu = 1 \dots N_p$,

$$z_i = \left(z_{i1}(t), \dots, z_{iN_p}(t) \right), \quad (34)$$

where N_p is the number of the parameters specifying each basis function,

$$g_i(x, t) := g_i(x, z_{i1}(t), \dots, z_{iN_p}(t)). \quad (35)$$

For simplicity, we assume here that N_b does not change in time, and that N_p is the same for all basis functions. The time-derivative of such a basis function is

$$\frac{dg_i}{dt} = \sum_{\mu=1}^{N_p} z_{i\mu} \frac{\partial g_i}{\partial z_{i\mu}}, \quad \dot{z} := \frac{dz}{dt}. \quad (36)$$

Substitution of Eqs (33) and (36) into the TDSE (1) and integration of the resulting expression multiplied by g_j over the coordinates space gives the following matrix equation:

$$i\hbar \mathcal{S} \frac{dc}{dt} = (\mathbf{H} - i\mathbf{D})c. \quad (37)$$

As in Section 3, \mathcal{S} is the overlap matrix, $S_{ij} = \langle g_i | g_j \rangle$; \mathbf{H} denotes the Hamiltonian matrix, $H_{ij} = K_{ij} + V_{ij}$,

$$K_{ij} = -\frac{1}{2} \left\langle g_i \left| \sum_{n=1}^f \frac{1}{m_n} \frac{\partial^2}{\partial x_n^2} \right| g_j \right\rangle, \quad V_{ij} = \langle g_i | V(x) | g_j \rangle. \quad (38)$$

The new matrix \mathbf{D} is the non-hermitian matrix, accounting for the time-dependence of the basis functions,

$$D_{ij} = \left\langle g_i \left| \sum_{\mu=1}^{N_p} \frac{d}{dt} z_{j\mu} \frac{\partial g_j}{\partial z_{j\mu}} \right| g_j \right\rangle. \quad (39)$$

Eq. (37) determines evolution of the expansion coefficients c , defining $\psi(x, t)$ in a basis influenced by an external, possibly time-dependent potential, V .

The choice of the time-dependence of the basis functions, i.e. of the parameters $z_i(t)$ (Eq. (34)), determines the accuracy and conservation properties of the dynamics. As shown, for example, in Ref. [67], the normalization of the wavefunction determined by Eq. (37) is conserved regardless of the quality of the basis representation or of the basis time-dependence. The total energy of a system,

$$E = \langle \psi(x, t) | \hat{H} | \psi(x, t) \rangle, \quad (40)$$

is conserved in three cases: (i) for *any* time-independent basis; (ii) for a time-dependent basis whose parameters are determined variationally, e.g. by applying the Dirac-Frenkel variational principle [68]; (iii) for a time-dependent basis which is *complete* in a sense of being sufficient to represent the wavefunction for a specific problem.

We have discussed the time-independent Gaussian bases, i.e. case (i), in Section 3. Out of the variational time-dependent basis methods, i.e. case (ii), the most relevant representative is the Gaussian-based vMCG method [69, 70, 71, 72]. It

has been noted, however, that the variational equations on the Gaussian parameters are ill-conditioned, and for general problems, the solutions become physically non-intuitive with time and are challenging to converge numerically [24, 73]. Limiting the Gaussian basis to the bath DOFs while using more conventional description for the active 'system' DOFs, has been shown a much more practical approach enabling challenging high-dimensional applications [25, 26, 74].

All-in-all, time-dependent bases whose parameters are not variational (case (iii)), but instead come from classical or semiclassical theories of motion, have been actively explored. As mentioned above, with this type of bases, the energy is not formally conserved, but this feature maybe used as in indicator of the basis completeness during the dynamics. The parameters of the non-variational Gaussian basis methods, many of which are developed for non-adiabatic dynamics on multiple coupled PESs, are defined by the positions and momenta of classical or Ehrenfest-type trajectories, often sampling the phase space of an initial wavefunction. One of such methods is the ab initio multiple spawning method, involving a GWP basis 'driven' by classical molecular dynamics, while additional GWPs are spawned during non-adiabatic events [75, 76, 77, 78]. This method is incorporated into MOLPRO [78] and large applications include chromophores in complex molecular environments [79]. The multiconfigurational Ehrenfest method developed by Shalashilin and co-workers on the basis of coupled coherent states expansions [80, 81, 82] utilizes bases simultaneously evolving on multiple electronic states according to the Ehrenfest dynamics.

The advantage of the methods with predefined time-dependence of the Gaussian basis functions, is that the remaining dynamics equations (37) for the expansion coefficients are much easier to implement numerically than the complete set of equations for the fully variational basis. The usual concern is that defining the basis functions through classical dynamics may miss regions of space, inaccessible to classical trajectories, but involved in exact quantum dynamics. Therefore, the *quantum* trajectories (QTs) representing a time-dependent wavefunction as a correlated ensemble provide have been considered as 'guides' for the Gaussian basis functions.

4.1.1 The quantum trajectory dynamics

The Madelung-de Broglie-Bohm, also referred to as the hydrodynamic or the QT, formulation of the TDSE [83, 84, 85] is based on the polar representation of a complex wavefunction, expressed in terms of real amplitude $\mathcal{A}(x, t)$ and phase $\mathcal{S}(x, t)$,

$$\psi(x, t) = \mathcal{A}(x, t) \exp\left(\frac{i}{\hbar} \mathcal{S}(x, t)\right). \quad (41)$$

Substitution of the ansatz (41) into TDSE (1) leads to the following time-dependence of the wavefunction phase \mathcal{S} and probability density ρ ,

$$\rho(x, t) = |\psi(x, t)|^2 = \mathcal{A}^2, \quad (42)$$

$$\frac{\partial \mathcal{S}}{\partial t} = -\frac{1}{2} \nabla^T \mathcal{S} \mathbf{M}^{-1} \nabla \mathcal{S} - V - U, \quad (43)$$

$$\frac{\partial \rho}{\partial t} = -\nabla^T \mathcal{S} \mathbf{M}^{-1} \nabla \rho - \rho \nabla^T \mathbf{M}^{-1} \nabla \mathcal{S}. \quad (44)$$

The time-dependent function $U \equiv U(x, t)$ denotes the *quantum* potential, as opposed to the *classical* potential V ,

$$U = -\frac{\hbar^2}{2\mathcal{A}} \nabla \mathbf{M}^{-1} \nabla \mathcal{A}. \quad (45)$$

To clarify the meaning of Eqs (43) and (44) let us switch to the language of the trajectory dynamics. The gradient of the wavefunction phase,

$$p(x, t) = \nabla \mathcal{S}(x, t), \quad (46)$$

at the position of the *quantum trajectory* x_t defines its momentum,

$$p_t = \nabla \mathcal{S}|_{x=x_t}, \quad \frac{dx_t}{dt} = \mathbf{M}^{-1} p_t. \quad (47)$$

Then, in the Lagrangian frame-of-reference,

$$\frac{d}{dt} = \frac{\partial}{\partial t} + \mathbf{M}^{-1} p_t^T \nabla, \quad (48)$$

one obtains the quantum Hamilton-Jacobi equation for the wavefunction phase \mathcal{S}_t , and the continuity equation for the probability density ρ_t ,

$$\frac{d\mathcal{S}_t}{dt} = \frac{1}{2} p_t^T \mathbf{M}^{-1} p_t - (V + U)|_{x=x_t}, \quad (49)$$

$$\frac{d\rho_t}{dt} = -\rho_t \nabla^T \mathbf{M}^{-1} p(x, t)|_{x=x_t}. \quad (50)$$

The equation of motion for p_t is obtained by transforming the gradient of Eq. (43) into the moving frame-of-reference defined by Eq. (48),

$$\frac{dp(x_t)}{dt} = -\nabla(V + U)|_{x=x_t}.$$

Comparison of the quantum Hamilton-Jacobi equation (49) to its classical counterpart shows that all 'quantumness' in the time-evolution of $\psi(x, t)$ is expressed through the potential-like function $U = U(x, t)$ in Eq. (45), known as the quantum potential [86]. The exponential scaling of quantum mechanics is traced to this non-local time-dependent function which, being added to the external classical potential V , generates the quantum features in dynamics. Certain simplifications, however, might be expected for heavy particles, such as nuclei: being inversely proportional to the particle mass, the quantum potential becomes negligible in the classical limit.

Therefore, nuclear motion may be treated as classical dynamics with quantum corrections due to the quantum potential [87, 88].

The efficiency of the QT description of a wavefunction follows from Eq. (50), according to which ρ within the volume element δx of each trajectory is conserved [87],

$$\rho(x, t) \delta x_t = \rho(x, 0) \delta x_0. \quad (51)$$

Thus, a single QT ensemble, accurately representing $\psi(x, 0)$, will remain adequate to represent $\psi(x, t)$ at all times. The exact QTs may be interpreted as a time-dependent grid optimized for a specific $\psi(x, t)$. The catch is that the numerical implementation of Eq. (49) is, in general, impractical: U becomes singular as $\psi(x, t) \rightarrow 0$. However, the QT dynamics may be used to define a nearly optimal time-dependent Gaussian basis, without solving the dynamics equations for QTs, which would require computation of the quantum potential. Instead, we define the QT momentum, p from the wavefunction represented in a basis via Eq. (33), and use it to update the trajectory positions, which serve as the centers of the Gaussian basis functions.

4.1.2 Quantum trajectory-guided basis of real frozen Gaussians

To implement the QT-guided Gaussian bases, we construct an adaptive basis out of time-dependent multidimensional Gaussians (d is the number of DOFs),

$$g_i = \sqrt[4]{\frac{\det \mathbf{A}}{\pi^d}} \exp \left(-\frac{1}{2} \sum_{n, n'=1}^d (x_n - q_{i_n}(t)) A_{nn'} (x_{n'} - q_{i_{n'}}(t)) \right). \quad (52)$$

The basis function g_i is centered at the position of the i^{th} quantum trajectory q_i , their number defining the size of the basis N_b . For simplicity, let us assume that the matrices \mathbf{A} and \mathbf{M} are diagonal, and their non-zero elements are $A_{nn} = \alpha_n$ and $M_{nn} = m_n$, respectively.

Note, that the Gaussian function of Eq. (52) above is different from the Gaussians of the Frozen Gaussian or Herman-Kluk semiclassical propagators [32, 34], which include linear in x phases, dependent on the momentum of a classical trajectory of the Gaussian center,

$$\mathcal{S}^{lin} = p_i(t) (x - q_i(t)) + \gamma_i(t).$$

In the real basis formulation the time-dependence of the expansions coefficients $c_i(t)$ incorporates the effect of $\gamma_i(t)$ associated with the classical action function at q_i . Restriction for the basis functions in Eq. (52) to be real simplifies the formalism and makes implementation more robust: there is no term dp/dt in Eq. (36), thus unstable computation of ∇U is not needed. Omitting time t in the argument of functions for clarity, the matrix elements of Eqs (39) and (38) are:

$$S_{ij} = \prod_{n=1}^d \exp \left(-\frac{\alpha_n}{4} (q_{i_n} - q_{j_n})^2 \right), \quad (53)$$

$$D_{ij} = \left\langle g_i \left| -i \frac{\partial}{\partial t} \right| g_j \right\rangle = \frac{i}{2} \sum_{n=1}^d \frac{\alpha_n}{m_n} p_{j_n} (q_{i_n} - q_{j_n}) S_{ij}. \quad (54)$$

The matrix elements for the kinetic energy operator are:

$$K_{ij} = \sum_{n=1}^d \frac{\alpha_n}{4m_n} \left(1 - \frac{\alpha_n}{2} (q_{i_n} - q_{j_n})^2 \right) S_{ij}. \quad (55)$$

The potential energy matrix elements in the examples below are evaluated within the local harmonic approximation to V at the midpoint \bar{q} of the Gaussian center q_i or q_j :

$$V_{ij} = \left(V(\bar{q}) + \sum_{n=1}^d \frac{1}{4\alpha_n} \frac{\partial^2 V(\bar{q})}{\partial x_n^2} \right) S_{ij}, \quad (56)$$

where $\bar{q} = (q_i + q_j)/2$. Some other PES approximations for evaluation of V_{ij} , balancing the accuracy and numerical cost are: a symmetric combination of the local harmonic approximations, a cheaper alternative for the *ab initio* PES evaluated on-the-fly; the linear local expansion of $V(\bar{q})$ (no second derivative of V) as in the coupled coherent Gaussians method [80]; the product-basis fit of the PES developed by the MCTDH community [27, 28, 89]; evaluation by quadrature. The QT position, i.e. the Gaussian center of the i^{th} function, is incremented at each time-step according to the momentum determined from $\psi(x, t)$:

$$\frac{d}{dt} q_{i_n} = \sum_{n=1}^d \frac{p_{i_n}}{m_n}, \quad p_i = \Im \left(\frac{\nabla \psi}{\psi} \right) \Big|_{x=q_i}. \quad (57)$$

In the *frozen* Gaussian implementation, outlined here, a QTGB simulation is started with the expansion of the initial wavefunction in terms of the Gaussian functions of fixed width α . Their centers are the initial positions of the QTs. The number of Gaussians, N_b , depends on the target accuracy. For high-dimensional systems the sampling of the initial QT positions is random or quasi-random. The initial momenta of QTs are defined by the initial wavefunction according to Eq. (57). The choice of α will affect the basis size and the accuracy of V_{ij} of Eq. (56) through the validity of the local harmonic (or other) approximation. Analogous to the QTGB approach of Section 3, the value of α and the density of the Gaussian centers should be such as to yield a reasonable condition number of the overlap matrix. Thus, it is necessary to try several values of α and basis size to assess convergence and the accuracy of the desired output quantities. The dynamics itself is accomplished by solving Eq. (37).

4.2 Implementation and model problems

In this subsection, we discuss certain aspects of implementation of the QTGB dynamics, which is then applied to several models: the Morse oscillator representing the vibration of H_2 , scattering on the Eckart barrier, the 1D and 2D double-well potentials. The exact quantum-mechanical results come from the split-operator propagation implemented on a grid [90, 91].

4.2.1 Implementation

As discussed in Section 3, Gaussian bases of strongly overlapping functions may lead to ill-conditioned overlap matrix \mathcal{S} , which in case of QTGB has to be inverted to solve Eq. (37). In dynamics this situation may emerge in the course of time-evolution [52]. Formally, the non-crossing property of the QTs mitigates this problem for QTGBs: exact QTs never cross due to the strongly repulsive quantum potential developing as the trajectories approach each other. In practice, however, this property makes the QT dynamics inherently unstable and, moreover, for the Gaussians of fixed width may become so close as to generate an ill-conditioned overlap matrix \mathcal{S} , indicating redundancy in a basis.

To deal with this problem, following Refs [92, 93, 94], we occasionally 'restart' the basis, by reexpanding $\psi(x, t)$ in a new set of Gaussian basis functions, i.e. $\psi(x, t)$ is re-sampled in terms of the new QT ensemble. The reexpansion procedure prevents Gaussians from colliding, removes basis functions in the regions of negligible probability density and adds more functions in the regions of increasing probability density. The exact QTs would track such changes in the probability density through the continuity equation (51). However, real frozen Gaussians do not have the flexibility to account for such changes, captured in QTGB by the expansion coefficients. Therefore, instantaneous adjustments of the basis increase accuracy and stability of the dynamics.

In the examples below we have used a simple reexpansion algorithm to generate equidistant distribution of Gaussian centers of the new basis. We identify the left-most outlying point q_1 . If the probability density at q_1 exceeds a predefined threshold ε ,

$$|\psi(q_1, t)|^2 = \left| \sum_i c_i g_i(q_1) \right|^2 > \varepsilon,$$

then q_1 is taken as a center of a Gaussian included in the new basis (or the next point q_2 is tested and so on). Moving to the right in position in increments of Δq , until the region of negligible density on the right is reached, generates additional basis functions. In high dimensionality a new set $\{q'_i\}$ can be generated through the random importance sampling, similar to the construction of QDGBs of Section 3. The size of the resulting new basis, N'_b , is generally different from the old N_b , which adapts the basis to the wavefunction localization. The new expansion coefficients, $\{c'_i\}$, are determined by minimization of the expansion error in the two bases,

$$I = \left\| \sum_i c'_i g'_i - \psi(x, t) \right\|^2. \quad (58)$$

The resulting matrix equation on $\{c'_i\}$ is,

$$\mathbf{S}' c' = b', \quad (59)$$

where

$$S'_{ij} = \langle g'_i | g'_j \rangle, \quad b'_i = \langle g'_i | \psi \rangle, \quad (60)$$

and $\psi(x, t)$ is expanded in the old basis, Eq. (33). The expansion coefficients are updated according to the second-order time differencing scheme [90],

$$c(t + \Delta t) = c(t - \Delta t) + 2\Delta t \frac{dc}{dt}, \quad (61)$$

with dc/dt defined by Eq. (37).

To start the dynamics in the new basis at time T , we have to assign momenta to the QTs of a new basis. According to Eq. (57), the QT momentum is the gradient of the phase of $\psi(x, T)$ evaluated at $x = q'_i$. To ensure smoothness of the momentum as a function of position for a *sparse* set of QTs, we use a convoluted wavefunction $\tilde{\psi}_\beta(x, t)$ as given below in one dimension:

$$\tilde{\psi}_\beta(x, t) = \left(\frac{\beta}{2\pi} \right)^{1/2} \int_{-\infty}^{\infty} e^{-\frac{\beta}{2}(x-y)^2} \psi(y, t) dy. \quad (62)$$

Using $\tilde{\psi}_\beta$ of Eq. (62) in Eq. (57), the momentum of the Gaussian center is:

$$p = - \left(\frac{\beta}{\pi} \right)^{1/4} \Im \left(\frac{\beta}{\psi(x, t)} \int_{-\infty}^{\infty} (x-y) e^{-\frac{\beta}{2}(x-y)^2} \psi(y, t) dy \right), \quad (63)$$

The integrals above are analytic. As $\beta \rightarrow \infty$, $\tilde{\psi}_\beta \rightarrow \psi$, and the convolution has no effect on p . If $\beta \rightarrow 0$, then the momenta of all trajectories approach the average value of p and deviate significantly from the QT momenta. To generate smooth $p(q_i)$, we select such values of β , so that several Gaussians make significant contribution to $\tilde{\psi}_\beta$ at each q_i . Note, that since the trajectory momenta p_i are not part of the basis function definition, the convolution procedure or other choices of the momenta do not affect the accuracy of the reexpansion. They will affect, however, the quality, i.e. completeness, of the basis at later times: having momenta closer to the QT values yields accurate basis representation of the wavefunction for longer times, while assigning all momenta equal values will, generally, necessitate frequent reexpansions to attain the desired accuracy.

4.2.2 Numerical examples

The QTGB method is illustrated here for the double-well potentials in one and two dimensions. Additional model systems are described in Ref. [95].

The double-well potential is a prototypical model of reactions in condensed phase. It is an important test for any dynamics methods, as it presents a major challenge for the trajectory-based semiclassical dynamics of light particles due to the population transfer between the wells via tunneling at low energies: the classical trajectories with energies below the barrier top can not overcome the barrier. Some of the quantum trajectories, however, gain energy from the QT ensemble and cross the barrier even if their initial energies are below the barrier top. The total energy of the QT ensemble, which fully describes $\psi(x, t)$, is conserved, but the energy of individual QTs is not and can be exchanged through the time-dependent quantum potential. Thus, ideally, in a double-well potential, the QT-guided Gaussian basis can be initially localized in the reactant well, yet describe the wavefunction density in the product well at a later time as the guiding QTs migrate to the product well. First we consider a 1D symmetric double-well potential modeling an electron transfer [92]:

$$V(x) = \frac{1}{16\zeta}x^4 - \frac{1}{2}x^2, \quad (64)$$

where $\zeta = 1.3544 a_0^4/E_h$. The barrier height is $V^\ddagger = 1.3544 E_h$. The initial wavefunction is a Gaussian wavepacket,

$$\psi(x, 0) = \sqrt[4]{\frac{2\alpha_0}{\pi}} \exp(-\alpha_0(x - q_0)^2 + ip_0(x - q_0)), \quad (65)$$

whose parameters are $\{\alpha_0 = 0.5, q_0 = -2.5, p_0 = 0\}$ in atomic units. The particle mass is $m = 1$, and the time-step is 0.001 atomic units. The Gaussian width parameters are $\{\alpha = 8, \beta = 2\} a_0^{-2}$. The wavefunction is localized in the left well. The wavefunction energy is about 2/3 of the barrier height. The barrier is wide: the distance between the two minima is around 4.7 a_0 . Thus, tunneling is essential for population transfer, which presents a challenge for semiclassical methods [92]. The QTGB dynamics begins with $N_b = 16$ basis functions. The reexpansion is performed every 1500 timesteps resulting in increase the basis size with time to $N_b = 23$. Figure 6 shows the wavefunction amplitude at $t = \{0, 1.5, 3.0, 4.5, 6.0\}$ a.u. in the process of population transfer with tunneling. The Gaussian centers $\{q_i\}$, i.e. the QT positions, are plotted in the figure along the x -axis as functions of time up to $t = 6.0$ a.u. Thanks to the continuity equation (51), their behavior along illustrates the adaptation of the basis and the effect of reexpansions. Around $t = 5.4$ a.u. one of the QTs goes around a node, i.e. $\psi(x, t) = 0$, associated with interference effect. At the node near $x = 1.5 a_0$ the wavefunction changes sign, leading to singularities in the quantum potential and a breakdown of the QT dynamics. In QTGB dynamics, however, the interference pattern is reproduced through superposition of the basis functions. To assess the accuracy once again the autocorrelation function, a phase-sensitive quantity, is calculated for $t = [0, 24]$ a.u. $C(t)$ is computed using Eq. (67),

thus, $\psi(x,t)$ was propagated up to $t = 12$ a.u. $|C(t)|$ is shown in Fig. 7. The reexpansion procedure specified by Eq. (58) has been carried out until the error dropped below 5×10^{-5} . The time-dependence of the total energy is given in Fig. 7(inset). As discussed at the beginning of this section, in dynamics with the time-dependent bases, the energy conservation correlates not only the the accuracy of numerical solution to Eq. (37) but, importantly, with the basis completeness. In this example, with the energy minimum of $V(x)$ shifted to zero, the wavefunction energy remains constant within 1 – 2% of its initial value.

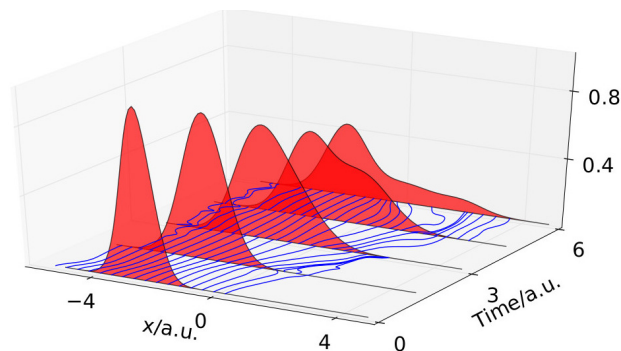
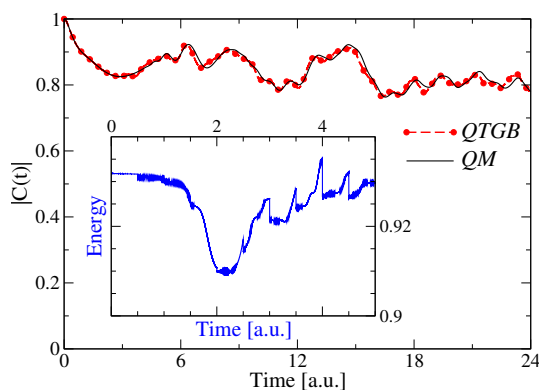


Fig. 6 QTGB dynamics in the one-dimensional double well. The blue lines mark the positions of the basis function centers $\{q\}_t$. The vertical axis represents the wavefunction amplitude, whose profiles are shown in red. The wavefunction has been reexpanded at $t = \{1.5, 3.0, 4.5\}$ a.u. The nodal pattern of the quantum trajectories going around the node at $x \approx 1.5 a_0$ is seen for $t \approx 5.4$ a.u. Adapted with permission from Ref. [95]. Copyright 2016 American Chemical Society.

Fig. 7 QTGB dynamics in the one-dimensional double well: the absolute value of the autocorrelation function, $C(t) = \langle \psi^2(x,t/2) \rangle$, is compared to the exact QM result. Inset: the total energy is conserved within 2% in the course of the QTGB dynamics. Adapted with permission from Ref. [95]. Copyright 2016 American Chemical Society.



Next, we examine the QTGB performance for a two-dimensional potential consisting of the double well linearly coupled to the harmonic oscillator of Ref. [96],

$$V(x_1, x_2) = x_2^2(\xi_1 x_2^2 - \xi_2) + \frac{1}{2}\xi_3(x_1 - x_2)^2 + \frac{\xi_2^2}{4\xi_1}. \quad (66)$$

The contour plot in Fig. 8 corresponds to the parameter values of $\xi_1 = 1$, $\xi_2 = 4$ and $\xi_3 = 4$. The minima of V are located at $(-\sqrt{2}, -\sqrt{2})$ and $(\sqrt{2}, \sqrt{2})$ a.u. The barrier top is $V^\dagger = 4$ a.u.

The wavefunction is initialized as the direct product of two Gaussians specified by Eq. (65), centered at the left-hand-side potential minimum. The parameters are listed in Table 3. In this model, we focus on the two lowest energy eigenvalues, extracted from the exact QM and QDGB dynamics from the spectrum of autocorrelation functions generated on the interval $t = [0, 6.0]$ a.u. Since the initial wavefunction is real, the correlation function is computed as

$$C(t) = \langle \psi_0 | e^{-i\hat{H}t} | \psi_0 \rangle = \int_{-\infty}^{\infty} \psi^2(x, t/2) dx, \quad (67)$$

and transformed into the energy domain using harmonic inversion to enhance the resolution of the spectral features [97, 98]. The eigenvalues presented in Table 3 have been obtained from dynamics performed with 10×10 , 12×12 and 16×16 basis functions. The positions of the Gaussian centers at $t = 3.0$ a.u. (see Fig. 8) illustrate the adaptation of the basis functions, initially centered on a square grid of positions $\{q_i\}$. The frequencies of the symmetric ground and first excited states are listed in Table 3,

$$\nu_{0(1)} \equiv \frac{E_{0(1)}}{2\pi},$$

and compared to the results from the conventional time-evolution on the spatial grid of 512×512 equidistant points. Calculations are performed with several sets of parameters listed in Table 3. The frequencies, which are very sensitive to the quality of the correlation function, agree with the QM results quite well.

In the 2D double well example the wavefunction reexpansion was not necessary, since the eigen-frequencies were obtained from short-time dynamics. In general, however, this procedure gives a practical way of reducing the basis size and of controlling accuracy of dynamics. The wavefunction reexpansions enable adaptation of the stationary Gaussian bases, which can be viewed as 'intermediate' between the time-dependent and time-independent representations. Several promising methods of this type are outlined in Section 5.

5 Time-sliced dynamics with stationary Gaussian bases

In quantum dynamics, the algorithms for expansion and reexpansion of wavefunctions in terms of Gaussian basis functions, are essential for practical treatment of delocalized wavefunctions, as it balances the basis size, accuracy and stability of the time-evolution. For several Gaussian basis methods discussed in this Section, the wavefunction reexpansion procedure is central to performing the dynamics. Two

Fig. 8 QTGB dynamics in the two-dimensional double-well potential: positions $\{q_1, q_2\}$ of the basis function centers, shown as circles at $t = 3.0$ a.u., are superimposed on the contour plot of $V(x_1, x_2)$ given by Eq. (66). The horizontal and vertical axes are the x_1 and x_2 coordinates/center positions in atomic units, respectively. Adapted with permission from Ref. [95]. Copyright 2016 American Chemical Society.

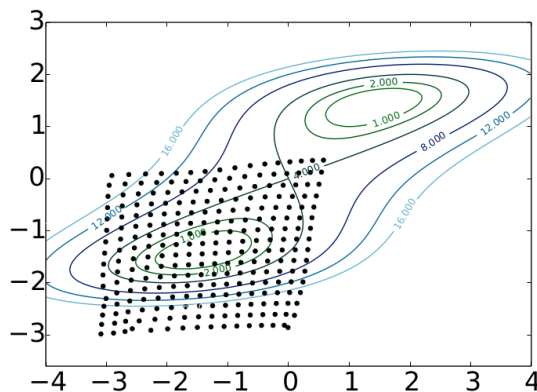


Table 3 The two-dimensional double-well model. The initial wavefunction and propagation parameters for three QTGB calculations, and the eigen-frequencies of the ground and first excited states are given in atomic units. The parameters α_0 , q_0 and p_0 are defined in Eq. (65). N_b and α is the number and width of the basis functions given Eq. (52).

Wavefunction and propagation parameters				
α_0	q_0	p_0	m	Δt
0.5	-1.4	0.0	1	0.001
QT-guided Gaussian Bases			exact QM	
α	16	16	32	
N_b	10×10	12×12	16×16	128×128
Frequencies [a.u.]				
ν_g	0.4827	0.4822	0.4830	0.4829
ν_e	0.7110	0.7180	0.7209	0.7163

earlier methods, i.e. Matching-Pursuit Split-operator Fourier-Transform [92, 99] and Quantum Wavepacket Ab Initio Molecular Dynamics [100, 101], combine exact short-time quantum evolution of the Gaussian basis functions with occasional re-expansions of a wavefunction in a new, presumably more efficient and accurate, Gaussian basis. The matching pursuit strategy is based on growing a 'new' basis by adding one basis function at a time. The functions are chosen, according to a certain algorithm, to minimize the residual difference between the wavefunction representations in the 'old' and the 'new' basis under construction, until the desired criterion is fulfilled. Thus, the basis is adjusted according to the time-evolution of a wavefunction encoded in the time-dependent expansion coefficients and in the parameters of the Gaussian basis functions.

More recent adaptable Gaussian-based methods, i.e. the basis expansion leaping multi-configurational Gaussians (BEL-MCG) of Frankcombe [93] and the trajectory-guided time-independent Gaussian basis of Saller and Habershon [94] forego the time-dependence of the basis functions altogether. In BEL-MCG just the basis reexpansion, or 'leaping', is left. The basis is stationary between the leaps,

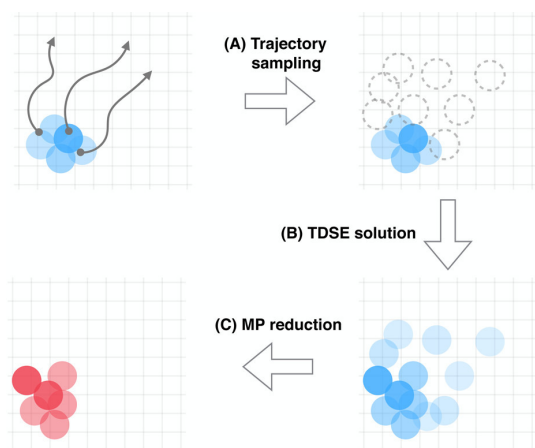
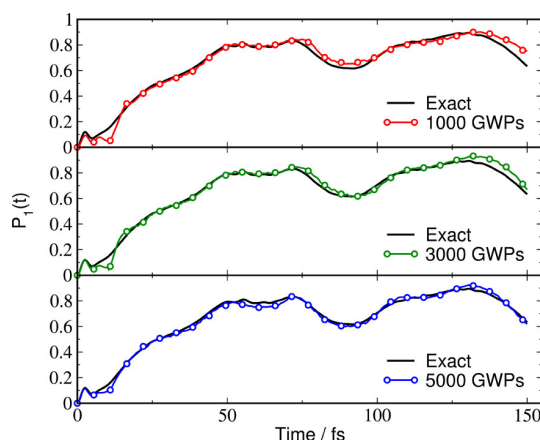


Fig. 9 The trajectory guiding algorithm. (A) An initial wavefunction is expanded in a basis of Gaussians (blue circles). Additional Gaussians (dashed circles) come from sampling of short-time classical trajectories (grey lines). (B) Solution of the TDSE within the full basis is followed by (C) the basis reduction deploying the matching pursuit method. The cycle closes when a time-evolved wavefunction is expressed in a new, compact basis of Gaussian functions (red circles). Adapted with permission from Ref. [102]. Copyright 2017 American Chemical Society.

and is adjusted at certain intervals of time by constructing a more compact basis to express the time-evolved wavefunction. The advantage of the approach is that the Hamiltonian and overlap matrices are evaluated only once per each time-interval between the leaps. In the work by Habershon and co-workers, the choice of the Gaussian parameters comes from the classically evolved trajectories, sampling the Wigner transform of the initial wavefunction. The classical trajectory dynamics allows one to anticipate where the basis functions will be needed in the course of quantum dynamics of the wavefunction, and thus to construct an adequate basis of stationary Gaussians, tuned to the upcoming dynamics, though certainly not a 'minimal' basis for problems undergoing large amplitude motion. The Hamiltonian and overlap matrices are computed just once, which is a very appealing feature if the PES evaluations are expensive. The downside is that classical trajectories may not cover certain regions of space, such as those accessed through the quantum tunneling. A very recent development of the trajectory-guided time-independent basis is to apply this idea to short segments of time to generate a compact adaptive basis [102]. The 'new' basis is constructed based on short-time classical trajectories, so the earlier deficiency of classical vs quantum spaces is mitigated. In addition, the basis functions of the 'old' basis with small expansion coefficients are removed at the reexpansion step, accomplished using the matching pursuit algorithm, to reduce the basis size. Figure 9 illustrates the method.

This time-sliced propagation scheme with basis adjustments allowed to reduce the basis size by an order of magnitude (compared to the original method of Ref. [94]) for challenging benchmark applications – for a 4-dimensional model of pho-

Fig. 10 Population of the lower diabatic S1 state, $P_1(t)$, as a function of time, calculated using adaptive basis sets with varying size, for the 4D pyrazine Hamiltonian. The basis set sizes given are approximately the number of GWPs which form the wave function during each short 10 fs propagation period. Adapted with permission from Ref. [102]. Copyright 2017 American Chemical Society.



toexcited pyrazine (shown in Fig. 10) and for a system tunneling in a double-well coupled to 2-20 harmonic DOFs representing the environment. In case of pyrazine, the time-slices are 10 fs, while the total propagation time is 150 fs long. Another promising combination of short time-evolution and basis reduction, is Time-Sliced Thawed Gaussian Propagation Method of Batista and co-workers [51]. In this method the basis functions evolve as TGWPs, and the segments are combined employing the Husimi transform in the limit of highly overlapping Gaussians, at which step functions with negligible contribution to the wavefunction are removed.

The emerging overall conclusion on the Gaussian basis representation of time-dependent wavefunctions is: the basis reexpansion is a useful tool of improving stability and accuracy of dynamics with the time-independent or time-dependent Gaussian bases. The basis reexpansion also helps to keep non-variational bases compact. The dynamics information, either from the time-dependent wavefunction itself, or from certain relevant exploratory trajectories, is beneficial for constructing physically meaningful, small yet accurate bases.

6 Summary and outlook

In this chapter we discussed Gaussian basis methods of solving the time-independent and time-dependent SE for the nuclei. The same ideas could be used to solve the SE for electrons, or for both nuclei and electrons. Extension to electrons may be desirable, for example, in the presence of the time-dependent electric field of a laser. We started by reviewing a time-dependent solution to SE for parabolic potentials, known as the thawed Gaussian wavepacket (TGWP) [31], when used with the local harmonic approximation to an arbitrary potential. A single complex TGWP is capable of describing mild quantum effects, associated with the wavepacket delocalization. In this regime the TGWP is sufficiently accurate and highly efficient as demonstrated by recent applications to spectroscopy of oligothiophenes and ammo-

nium inversion [42, 43]. It is particularly appealing, when combined with on-the-fly ab initio electronic structure calculations, as information on the PES and its gradients is needed along a *single* classical trajectory. In more challenging applications, the TGWPs have been successfully used to represent environmental DOFs, while more accurate basis representations are employed for the reactive modes [44, 45]. More generally, the idea of using classical trajectory information, such as energy and phase space analysis, to construct compact efficient basis representations has been incorporated into many exact QM dynamics methods, including time-independent, time-dependent and in-between approaches.

Out of time-independent methods, i.e. those based on Hamiltonian matrix diagonalization, we have reviewed a quasirandom distributed Gaussian bases (QDGBs). The advantage of QDGB is that it is correlated and adapted to a given PES. Checking convergence of eigenvalues, while the basis is constructed, is an advantage for high-dimensional studies whose feasibility is determined by the basis size. Some other notable developments of the Gaussian basis methodology in time-independent context, include phase space Gaussians on the von Neumann lattice with periodic boundary conditions [103, 104], and the wavelets representation obtained through canonical orthogonalization of the coherent state Gaussians [105]. Subsequent advances of the wavelets methodology (the truncation scheme and the momentum-symmetrized Gaussian basis) [106, 107] culminate in applications to acetonitrile (CH_3CN) and benzene, yielding thousands of eigenenergies [108, 109]. In the study of the benzene molecule, a 30 DOF problem, 500,000 eigenenergies below 6500 cm^{-1} were converged within 15 cm^{-1} . The approach is implemented in a massively parallel code SwitchBLADE, which is available for general use.¹

Next, we described construction of compact time-dependent Gaussian bases (GB), guided by the quantum-like trajectories (QT). From the properties of QTs, it follows that the basis functions track the flow of the probability density, providing in a sense the optimal in coordinates space time-dependent grid, and adapt to the dynamics of a specific wavefunction. Therefore, for problems characterized by large amplitude motion in selected DOFs, the scaling properties of QTGB with the system size should be superior to those of conventional time-independent bases. Time-evolution of QTs in the exact limit of strongly quantum dynamics is, generally, unstable, due to singular features in the quantum potential, responsible for the formal exponential scaling of complexity with the systems size [86]. Yet the trajectory framework is useful for quantum dynamics close to the classical regime, appropriate for the nuclei of polyatomic systems. In the QTGB approach, which is developed for this regime, the QTs move according to the momentum reconstructed from the wavefunction expanded in a Gaussian basis. Moreover, for real Gaussian basis functions, one can use modified QT momenta without making approximations, to improve the stability of propagation. The ensuing loss of efficiency is compensated by occasional reexpansions, performed to maintain completeness of the basis in time. The total wavefunction energy, which is rigorously conserved in the limit of a complete time-dependent basis, serves as a convenient measure of the basis

¹ Interested researchers should send their request to Bill Poirier at e-mail: Bill.Poirier@ttu.edu.

completeness and a criterion for the wavefunction reexpansion. So far, the QTGB method has been tested on low-dimensional model problems. We plan to extend QTGB to real Gaussians with adjustable width, and to improve the reexpansion procedure using ideas of matching pursuit and exploratory trajectory dynamics of Refs [92, 93, 102]. Though seemingly technical, the wavefunction reexpansion is at the core of the 'intermediate' between the time-dependent and time-independent Gaussian bases, i.e. the stationary Gaussian bases adapted to the evolving wavefunction at the reexpansion stage. All-in-all, non-variational dynamics-guided Gaussian bases, combined with recent advances in the on-the-fly electronic structure calculation, is a promising practical approach to perform quantum dynamics of large molecular systems.

Acknowledgements The author thanks John Light, Vitaly Rassolov and Bing Gu for collaborative research in the area of quantum trajectory and Gaussian basis dynamics. The author thanks Jiri Vanicek and Scott Habershon for permission to use some of their figures. This material is based upon work supported by the National Science Foundation under Grant No CHE-1056188, CHE-1565985 and OIA-1655740, and by a grant from the US Department of Energy, DE-FG02-87ER13679.

References

1. Kenji Sumida, David Stueck, Lorenzo Mino, Jeng-Da Chai, Eric D. Bloch, Olena Zavorotynska, Leslie J. Murray, Mircea Dinca, Sachin Chavan, Silvia Bordiga, Martin Head-Gordon, and Jeffrey R. Long. Impact of Metal and Anion Substitutions on the Hydrogen Storage Properties of M-BTT Metal-Organic Frameworks. *J. Am. Chem. Soc.*, 135(3):1083–1091, JAN 23 2013.
2. Ming Shao, Jong Keum, Jihua Chen, Youjun He, Wei Chen, James F. Browning, Jacek Jakowski, Bobby G. Sumpter, Ilia N. Ivanov, Ying-Zhong Ma, Christopher M. Rouleau, Sean C. Smith, David B. Geohegan, Kunlun Hong, and Kai Xiao. The isotopic effects of deuteration on optoelectronic properties of conducting polymers. *Nature Commun.*, 5:3180, January 24 2014.
3. Weizhao Cai, Mihindra Dunuwille, Jiangang He, Trevor V. Taylor, Jasmine K. Hinton, Mary C. MacLean, Jamie J. Molaison, Antonio M. dos Santos, Stanislav Sinogeikin, and Shanti Deemyad. Deuterium isotope effects in polymerization of benzene under pressure. *J. Phys. Chem. Lett.*, 8(8):1856–1864, 2017. PMID: 28395511.
4. Tho D. Nguyen, T. P. Basel, Y. J. Pu, X-G. Li, E. Ehrenfreund, and Z. V. Vardeny. Isotope effect in the spin response of aluminum tris(8-hydroxyquinoline) based devices. *PHYSICAL REVIEW B*, 85(24), JUN 20 2012.
5. Judith P. Klinman and Adam R. Offenbacher. Understanding biological hydrogen transfer through the lens of temperature dependent kinetic isotope effects. *Accounts of Chemical Research*, 51(9):1966–1974, 2018.
6. D Kosloff and R Kosloff. A Fourier method solution for the time-dependent Schrodinger equation as a tool in molecular dynamics. *J. Comp. Phys.*, 52(1):35–53, 1983.
7. C Leforestier, RH Bisseling, C Cerjan, MD Feit, R Friesner, A Guldberg, A Hammerich, G Jolicard, W Karrlein, HD Meyer, N Lipkin, O Roncero, and R Kosloff. A Comparison of different propagation schemes for the time-dependent Schrodinger equation. *J. Comp. Phys.*, 94(1):59–80, MAY 1991.
8. R Kosloff. The Fourier Method. In Cerjan, C, editor, *Numerical grid methods and their applications to Schrodinger equation*, volume 412 of *NATO ADVANCED SCIENCE INSTI-*

- TUTES SERIES, SERIES C, MATHEMATICAL AND PHYSICAL SCIENCES*, pages 175–194. NATO, SCI COMM, 1993. NATO Advanced Research Workshop on Grid Methods in Atomic and Molecular Quantum Calculations, Corte, Fracne, Sep 27-Oct 03, 1992.
9. R Kosloff. Propagation methods for quantum molecular dynamics. *Ann. Rev. Phys. Chem.*, 45:145–178, 1994.
 10. SR Billeter and WF VanGunsteren. A comparison of different numerical propagation schemes for solving the time-dependent Schrodinger equation in the position representation in one dimension for mixed quantum- and molecular dynamics simulations. *Molecular Simulation*, 15(5):301–322, 1995.
 11. Heather R. W. and Light J. C. Discrete variable theory of triatomic photodissociation. *J. Chem. Phys.*, 79:147, 1983.
 12. Light J. C., Hamilton I. P., and Lill J. V. Generalized discrete variable representation in quantum mechanics. *J. Chem. Phys.*, 82:1400, 1985.
 13. Lill J. V., Parker G. A., and Light J. C. The discrete variable finite basis approach to quantum scattering. *J. Chem. Phys.*, 85:900, 1986.
 14. J. C. Light and T. Carrington, Jr. Discrete variable representations and their utilization. *Adv. Chem. Phys.*, 114:263–310, 2000.
 15. C. Lanczos. An iteration method for the solution of the eigenvalue problem of linear differential and integral operators. *J. Research of the National Bureau of Standards*, 45:255–282, 1950. Research Paper 2133.
 16. Park T. J. and Light J. C. Unitary quantum time evolution by iterative lanczos reduction. *J. Chem. Phys.*, 85:5870, 1986.
 17. P. N. Roy and T. Carrington Jr. A direct-operation lanczos approach for calculating energy levels. *Chem. Phys. Lett.*, 257:98–104, 1996.
 18. A. Viel and C. Leforestier. Six-dimensional calculation of the vibrational spectrum of the hfco molecule. *J. Chem. Phys.*, 112:1212–1220, 2000.
 19. F. Gatti, B. Lasorne, and A. Meyer, H.-D. and Nauts. *Applications of Quantum Dynamics in Chemistry*. Springer, 2017.
 20. H. D. Meyer, U. Manthe, and L. S. Cederbaum. The multi-configurational time-dependent hartree approach. *Chem. Phys. Lett.*, 165(1):73 – 78, 1990.
 21. I. Burghardt, H.-D. Meyer, and L. S. Cederbaum. Approaches to the approximate treatment of complex molecular systems by the multiconfiguration time-dependent hartree method. *J. Chem. Phys.*, 111(7):2927–2939, 1999.
 22. H. D. Meyer and G. A. Worth. Quantum molecular dynamics: propagating wavepackets and density operators using the multiconfiguration time-dependent Hartree method. *Theor. Chem. Acc.*, 109:251–267, 2003.
 23. H. B. Wang and M. Thoss. Multilayer formulation of the multiconfiguration time-dependent Hartree theory. *J. Chem. Phys.*, 119:1289–1299, 2003.
 24. I. Burghardt, M. Nest, and G. A. Worth. Multiconfigurational system-bath dynamics using gaussian wave packets: Energy relaxation and decoherence induced by a finite-dimensional bath. *J. Chem. Phys.*, 119(11):5364–5378, 2003.
 25. S. Roemer, M. Ruckebauer, and I. Burghardt. Gaussian-based multiconfiguration time-dependent Hartree: A two-layer approach. I. Theory. *J. Chem. Phys.*, 138(6), FEB 14 2013.
 26. S. Roemer and I. Burghardt. Towards a variational formulation of mixed quantum-classical molecular dynamics. *Mol. Phys.*, 111(22-23, SI):3618–3624, DEC 1 2013.
 27. A Jackle and HD Meyer. Product representation of potential energy surfaces. *J. Chem. Phys.*, 104(20):7974–7984, MAY 22 1996.
 28. A Jackle and HD Meyer. Product representation of potential energy surfaces. II. *J. Chem. Phys.*, 109(10):3772–3779, SEP 8 1998.
 29. Richard Dawes, Alessio Passalacqua, Albert F. Wagner, Thomas D. Sewell, Michael Minkoff, and Donald L. Thompson. Interpolating moving least-squares methods for fitting potential energy surfaces: Using classical trajectories to explore configuration space. *The Journal of Chemical Physics*, 130(14):144107, 2009.

30. Gareth W. Richings and Scott Habershon. Direct quantum dynamics using grid-based wave function propagation and machine-learned potential energy surfaces. *Journal of Chemical Theory and Computation*, 0(0):null, 0.
31. Daniel Huber and Eric J. Heller. Generalized gaussian wave packet dynamics. *J. Chem. Phys.*, 87(9):5302–5311, 1987.
32. E. J. Heller. Frozen Gaussians: A very simple semiclassical approximation. *J. Chem. Phys.*, 75:2923, 1981.
33. E. J. Heller. Cellular dynamics - a new semiclassical approach to time-dependent quantum mechanics. *J. Chem. Phys.*, 94:2723–2729, 1991.
34. Michael F. Herman and Edward Kluk. A semiclassical justification for the use of non-spreading wavepackets in dynamics calculations. *Chemical Physics*, 91(1):27 – 34, 1984.
35. D. E. Skinner and W. H. Miller. Application of the semiclassical initial value representation and its linearized approximation to inelastic scattering. *Chem. Phys. Lett.*, 399:20–26, 1999.
36. D. J. Tannor. *Introduction to Quantum Mechanics: A Time-Dependent Perspective*. University Science Books, 2006.
37. E. Faou, V. Gradinaru, and C. Lubich. Computing semiclassical quantum dynamics with hagedorn wavepacketsal quantum dynamics with hagedorn wavepackets. *SIAM J. Sci. Comput.*, 31:3027, 2009.
38. E. J. Heller. Time-dependent approach to semiclassical dynamics. *J. Chem. Phys.*, 62:1544, 1975.
39. E. J. Heller. Wigner phase space method: Analysis for semiclassical applications. *J. Chem. Phys.*, 65:1289–1298, 1976.
40. R. D. Coalson and M. Karplus. Multidimensional variational Gaussian wave packet dynamics with application to photodissociation spectroscopy. *J. Chem. Phys.*, 93:3919–3930, 1990.
41. A. McLachlan. A variational solution of the time-dependent schrodinger equation. *Mol. Phys.*, 8:39, 1964.
42. M. Wehrle, M. Sulc, and J. Vanicek. On-the-fly ab initio semiclassical dynamics: Identifying degrees of freedom essential for emission spectra of oligothiophenes. *J. Chem. Phys.*, 140:244114, 2014.
43. Marius Wehrle, Solene Oberli, and Jiri Vanicek. On-the-Fly ab Initio Semiclassical Dynamics of Floppy Molecules: Absorption and Photoelectron Spectra of Ammonia. *J. Phys. Chem. A*, 119:5685–5690, 2015.
44. S Romer and I Burghardt. Towards a variational formulation of mixed quantum-classical molecular dynamics. *Mol. Phys.*, 111:3618, 2013.
45. S Romer, M. Ruckebauer, and I Burghardt. Gaussian-based multiconfiguration time-dependent hartree: A two-layer approach. i. *Theory. J. Chem. Phys.*, 138:064106, 2013.
46. R. C. Brown and E. J. Heller. Classical trajectory approach to photodissociation: The Wigner method. *J. Chem. Phys.*, 75:186–188, 1981.
47. K. G. Kay. Integral expressions for the semiclassical time-dependent propagator. *J. Chem. Phys.*, 100:4377–4392, 1994.
48. K. G. Kay. Semiclassical propagation for multidimensional systems by an initial-value method. *J. Chem. Phys.*, 101:2250–2260, 1994.
49. N. Makri and W. H. Miller. Coherent state semiclassical initial value representation for the Boltzmann operator in thermal correlation functions. *J. Chem. Phys.*, 116:9207–9212, 2002.
50. J. Liu and W. H. Miller. Linearized semiclassical initial value time correlation functions using the thermal Gaussian approximation: Applications to condensed phase systems. *J. Chem. Phys.*, 127(11):114506, 2007.
51. Xiangmeng Kong, Andreas Markmann, and Victor S. Batista. Time-sliced thawed gaussian propagation method for simulations of quantum dynamics. *The Journal of Physical Chemistry A*, 120(19):3260–3269, 2016.
52. MJ Davis and EJ Heller. Semi-classical Gaussian-basis set method for molecular vibrational wave-functions . *J. Chem. Phys.*, 71(8):3383–3395, 1979.
53. I. P. Hamilton and J. C. Light. On distributed gaussian bases for simple model multidimensional vibrational problems. *J. Chem. Phys.*, 84:306, 1986.

54. Z. Bacic and J. C. Light. Highly excited vibrational levels of floppy triatomic molecules: A discrete variable representation–distributed gaussian basis approach. *J. Chem. Phys.*, 85:4594, 1986.
55. Z. Bacic, R. M. Whitnell, D. Brown, and J. C. Light. Localized representations for large amplitude molecular vibrations. *Computer Phys. Commun.*, 51:35, 1988.
56. Z. Bacic, D. Watt, and J. C. Light. A variational localized representation calculation of the vibrational levels of the water molecule up to $27\,000\text{ cm}^{-1}$. *The Journal of Chemical Physics*, 89(2):947–955, 1988.
57. Andrew C. Peet. The use of distributed gaussian basis sets for calculating energy levels of weakly bound complexes. *The Journal of Chemical Physics*, 90(8):4363–4369, 1989.
58. Z. Bacic and J. C. Light. Theoretical methods for rovibrational states of floppy molecules. *Ann. Rev. Phys. Chem.*, 40:469, 1989.
59. Mirjana Mladenovic and Stefan Schmatz. Theoretical study of the rovibrational energy spectrum and the numbers and densities of bound vibrational states for the system $\text{hco}^+/\text{hoc}^+$. *The Journal of Chemical Physics*, 109(11):4456–4470, 1998.
60. Bill Poirier and J. C. Light. Efficient distributed gaussian basis for rovibrational spectroscopy calculations. *The Journal of Chemical Physics*, 113(1):211–217, 2000.
61. S. Garashchuk and J. C. Light. Quasirandom distributed Gaussian bases for bound problems. *J. Chem. Phys.*, 114:3929–3939, 2001.
62. W. H. Press, B. P. Flannery, S. A. Teukolsky, and W. T. Vetterling. *Numerical Recipes: The Art of Scientific Computing*. Cambridge University Press, Cambridge, 2 edition, 1992.
63. O. L. Polansky, P. J. Jensen, and J. Tennyson. The potential energy surface of H_2^16O . *J. Chem. Phys.*, 105:6490–6497, 1996.
64. Seung E. Choi and John C. Light. Highly excited vibrational eigenstates of nonlinear triatomic molecules: Applications to H_2O . *J. Chem. Phys.*, 97:7031, 1992.
65. Z. Bacic and J. C. Light. Accurate localized and delocalized vibrational states of hcn/hnc . *The Journal of Chemical Physics*, 86(6):3065–3077, 1987.
66. J. C. Light and Z. Bacic. Adiabatic approximation and nonadiabatic corrections in the discrete variable representation: Highly excited vibrational states of triatomic molecules. *The Journal of Chemical Physics*, 87(7):4008–4019, 1987.
67. Scott Habershon. Linear dependence and energy conservation in Gaussian wavepacket basis sets. *J. Chem. Phys.*, 136(1), JAN 7 2012.
68. J. Broeckhove, L. Lathouwers, E. Kesteloot, and P. V Leuven. On the equivalence of time-dependent variational principles. *Chem. Phys. Lett.*, 149:547, 1988.
69. I. Burghardt, H.-D. Meyer, and L. S Cederbaum. Approaches to the approximate treatment of complex molecular systems by the multiconfiguration time-dependent hartree method. *J. Chem. Phys.*, 111:2927, 1999.
70. G. A. Worth and I Burghardt. Full quantum mechanical molecular dynamics using gaussian wavepackets. *Chem. Phys. Lett.*, 368:502, 2003.
71. G. A. Worth, M. A. Robb, and I Burghardt. A novel algorithm for non-adiabatic direct dynamics using variational gaussian wavepackets. *Faraday Discuss.*, 127:307, 2004.
72. I. Burghardt, K. Giri, and G. A Worth. Multimode quantum dynamics using gaussian wavepackets: The gaussian-based multiconfiguration time-dependent hartree (g-mctdh) method applied to the absorption spectrum of pyrazine. *J. Chem. Phys.*, 129:174104, 2008.
73. D. V. Shalashilin and I. Burghardt. Gaussian-based techniques for quantum propagation from the time-dependent variational principle: Formulation in terms of trajectories of coupled classical and quantum variables. *J. Chem. Phys.*, 129(8):084104, 2008.
74. G.W. Richings, I. Polyak, K.E. Spinlove, G.A. Worth, I. Burghardt, and B. Lasorne. Quantum dynamics simulations using gaussian wavepackets: the vmcg method. *International Reviews in Physical Chemistry*, 34(2):269–308, 2015.
75. M. Ben-Nun and T. J. Martínez. A multiple spawning approach to tunneling dynamics. *J. Chem. Phys.*, 112(14):6113–6121, 2000.
76. M. Ben-Nun, J. Quenneville, and T. J. Martinez. Ab initio multiple spawning: Photochemistry from first principles quantum molecular dynamics. *J. Chem. Phys.*, 104:5161–5175, 2001.

77. A. Toniolo, C. Ciminelli, M. Persico, and T. J. Martínez. Simulation of the photodynamics of azobenzene on its first excited state: Comparison of full multiple spawning and surface hopping treatments. *J. Chem. Phys.*, 123(23):234308, 2005.
78. B. G. Levine, J. D. Coe, A. M. Virshup, and T. J. Martinez. Implementation of ab initio multiple spawning in the Molpro quantum chemistry package. *Chem. Phys.*, 347(1-3):3 – 16, 2008.
79. S. Olsen, K. Lamothe, and T. J. Martinez. Protonic Gating of Excited-State Twisting and Charge Localization in GFP Chromophores: A Mechanistic Hypothesis for Reversible Photoswitching. *J. Am. Chem. Soc.*, 132:1192+, 2010.
80. D. V. Shalashilin and M. S. Child. Real time quantum propagation on a Monte Carlo trajectory guided grids of coupled coherent states: 26D simulation of pyrazine absorption spectrum. *J. Chem. Phys.*, 121:3563–3568, 2004.
81. D. V. Shalashilin. Nonadiabatic dynamics with the help of multiconfigurational ehrenfest method: Improved theory and fully quantum 24d simulation of pyrazine. *J. Chem. Phys.*, 132:244111, 2010.
82. D. V. Makhov, W. J. Glover, T. J. Martinez, and D. V. Shalashilin. Ab initio multiple cloning algorithm for quantum nonadiabatic molecular dynamics. *J. Chem. Phys.*, 141:054110, 2014.
83. E. Madelung. Quantum theory in hydrodynamic form. *Z. Phys.*, 40:322–326, 1927.
84. L. de Broglie. *An introduction to the study of wave mechanics*. E. P. Dutton and Company, Inc.: New York, 1930.
85. D. Bohm. A suggested interpretation of the quantum theory in terms of "hidden" variables, I and II. *Phys. Rev.*, 85:166–193, 1952.
86. S. Garashchuk and V. A. Rassolov. Stable long-time semiclassical description of zero-point energy in high-dimensional molecular systems. *J. Chem. Phys.*, 129:024109, 2008.
87. S. Garashchuk and V. A. Rassolov. Energy conserving approximations to the quantum potential: Dynamics with linearized quantum force. *J. Chem. Phys.*, 120:1181–1190, 2004.
88. Sophya Garashchuk, Vitaly Rassolov, and Oleg Prezhdo. *Reviews in Computational Chemistry*, volume 27, chapter Semiclassical Bohmian dynamics, pages 111–210. Wiley, 2011.
89. Frank Otto. Multi-layer Potfit: An accurate potential representation for efficient high-dimensional quantum dynamics. *J. Chem. Phys.*, 140(1), JAN 7 2014.
90. R. Kosloff. Time-dependent quantum-mechanical methods for molecular dynamics. *J. Phys. Chem.*, 92:2087–2100, 1988.
91. M. D. Feit, J. A. Fleck Jr., and A. Steiger. Solution of the Schrödinger equation by a spectral method. *J. Comp. Phys.*, 47:412 – 433, 1982.
92. Y. H. Wu and V. S. Batista. Matching-pursuit for simulations of quantum processes. *J. Chem. Phys.*, 118:6720–6724, 2003.
93. Werner Koch and Terry J. Frankcombe. Basis Expansion Leaping: A New Method to Solve the Time-Dependent Schrodinger Equation for Molecular Quantum Dynamics. *Phys. Rev. Lett.*, 110(26), JUN 26 2013.
94. Maximilian A. C. Saller and Scott Habershon. Basis set generation for quantum dynamics simulations using simple trajectory-based methods. *Journal of Chemical Theory and Computation*, 11(1):8–16, 2015.
95. Bing Gu and Sophya Garashchuk. Quantum dynamics with gaussian bases defined by the quantum trajectories. *J. Phys. Chem. A*, 120(19):3023–3031, 2016.
96. S. Garashchuk, D. Dell’Angelo, and V. A. Rassolov. Classical limit of quantum nuclear dynamics based on selective use of the quantum potential. *J. Chem. Phys.*, 141:234107, 2014.
97. Vladimir A. Mandelshtam and Howard S. Taylor. Harmonic inversion of time signals and its applications. *J. Chem. Phys.*, 107:6756–6769, 1997.
98. V. A. Mandelshtam and H. S. Taylor. Harmonic inversion of time signals and its applications (vol 107, pg 6756, 1997). *J. Chem. Phys.*, 109:4128–4128, 1998.
99. X. Chen, Y. H. Wu, and V. S. Batista. Matching-pursuit/split-operator-Fourier-transform computations of thermal correlation functions. *J. Chem. Phys.*, 122(6), FEB 8 2005.
100. S. S. Iyengar and J. Jakowski. Quantum wave packet ab initio molecular dynamics: An approach to study quantum dynamics in large systems. *J. Chem. Phys.*, 122(11), 2005.

101. Jacek Jakowski, Isaiah Sumner, and Srinivasan S. Iyengar. Computational improvements to quantum wave packet ab initio molecular dynamics using a potential-adapted, time-dependent deterministic sampling technique. *J. Chem. Theory Comput.*, 2(5):1203–1219, 2006.
102. Maximilian A. C. Saller and Scott Habershon. Quantum dynamics with short-time trajectories and minimal adaptive basis sets. *Journal of Chemical Theory and Computation*, 13(7):3085–3096, 2017.
103. Asaf Shimshovitz and David J. Tannor. Phase-Space Approach to Solving the Time-Independent Schrodinger Equation. *Phys. Rev. Lett.*, 109(7), AUG 17 2012.
104. Shai Machnes, Elie Assémat, Henrik R. Larsson, and David J. Tannor. Quantum dynamics in phase space using projected von neumann bases. *The Journal of Physical Chemistry A*, 120(19):3296–3308, 2016.
105. B Poirier. Using wavelets to extend quantum dynamics calculations to ten or more degrees of freedom. *J. Theor. Comput. Chem.*, 2(1):65–72, MAR 2003.
106. B Poirier and A Salam. Quantum dynamics calculations using symmetrized, orthogonal Weyl-Heisenberg wavelets with a phase space truncation scheme. II. Construction and optimization. *J. Chem. Phys.*, 121(4):1690–1703, JUL 22 2004.
107. Thomas Halverson and Bill Poirier. Accurate quantum dynamics calculations using symmetrized Gaussians on a doubly dense Von Neumann lattice. *J. Chem. Phys.*, 137(22), DEC 14 2012.
108. Thomas Halverson and Bill Poirier. Large scale exact quantum dynamics calculations: Ten thousand quantum states of acetonitrile. *Chem. Phys. Lett.*, 624:37–42, MAR 16 2015.
109. Thomas Halverson and Bill Poirier. One million quantum states of benzene. *The Journal of Physical Chemistry A*, 119(50):12417–12433, 2015.